University Library

MINERVA ACCESS

A gateway to Melbourne's research publications

Minerva Access is the Institutional Repository of The University of Melbourne

Author/s:
Marques, FZ;Prestes, PR;Byars, SG;Ritchie, SC;Würtz, P;Patel, SK;Booth, SA;Rana, I;Minoda, Y;Berzins, SP;Curl, CL;Bell, JR;Wai, B;Srivastava, PM;Kangas, AJ;Soininen, P;Ruohonen, S;Kähönen, M;Lehtimäki, T;Raitoharju, E;Havulinna, A;Perola, M;Raitakari, O;Salomaa, V;Ala-Korpela, M;Kettunen, J;McGlynn, M;Kelly, J;Wlodek, ME;Lewandowski, PA;Delbridge, LM;Burrell, LM;Inouye, M;Harrap, SB;Charchar, FJ

Title:
Experimental and Human Evidence for Lipocalin-2 (Neutrophil Gelatinase-Associated Lipocalin [NGAL]) in the Development of Cardiac Hypertrophy and Heart Failure

Date:
2017-01-01

Citation:
Marques, F. Z., Prestes, P. R., Byars, S. G., Ritchie, S. C., Würtz, P., Patel, S. K., Booth, S. A., Rana, I., Minoda, Y., Berzins, S. P., Curl, C. L., Bell, J. R., Wai, B., Srivastava, P. M., Kangas, A. J., Soininen, P., Ruohonen, S., Kähönen, M., Lehtimäki, T. ,... Charchar, F. J. (2017). Experimental and Human Evidence for Lipocalin-2 (Neutrophil Gelatinase-Associated Lipocalin [NGAL]) in the Development of Cardiac Hypertrophy and Heart Failure. Journal of the American Heart Association, 6 (6), https://doi.org/10.1161/JAHA.117.005971.

Persistent Link:
https://hdl.handle.net/11343/213539

License:
CC BY-NC

ORIGINAL RESEARCH

Experimental and Human Evidence for Lipocalin-2 (Neutrophil Gelatinase-Associated Lipocalin [NGAL]) in the Development of Cardiac Hypertrophy and Heart Failure

Francine Z. Marques, MSc, PhD; Priscilla R. Prestes, MSc; Sean G. Byars, PhD; Scott C. Ritchie, MSc; Peter Würtz, PhD; Sheila K. Patel, PhD; Scott A. Booth, BSc; Indrajeetsinh Rana, PhD; Yosuke Minoda, BSc; Stuart P. Berzins, PhD; Claire L. Curl, PhD; James R. Bell, PhD; Bryan Wai, MBBS; Piyush M. Srivastava, MBBS; Antti J. Kangas, MSc; Pasi Soininen, PhD; Saku Ruohonen, PhD; Mika Kähönen, MD, PhD; Terho Lehtimäki, MD, PhD; Emma Raitoharju, PhD; Aki Havulinna, MSc; Markus Perola, MD, PhD; Olli Raitakari, MD, PhD; Veikko Salomaa, MD, PhD; Mika Ala-Korpela, PhD; Johannes Kettunen, PhD; Maree McGlynn, BSc; Jason Kelly, BSc; Mary E. Wlodek, PhD; Paul A. Lewandowski, PhD; Lea M. Delbridge, PhD; Louise M. Burrell, MBChB, PhD; Michael Inouye, PhD;* Stephen B. Harrap, MBBS, PhD;* Fadi J. Charchar, PhD*

***Background*—**Cardiac hypertrophy increases the risk of developing heart failure and cardiovascular death. The neutrophil inflammatory protein, lipocalin-2 (LCN2/NGAL), is elevated in certain forms of cardiac hypertrophy and acute heart failure. However, a specific role for LCN2 in predisposition and etiology of hypertrophy and the relevant genetic determinants are unclear. Here, we defined the role of LCN2 in concentric cardiac hypertrophy in terms of pathophysiology, inflammatory expression networks, and genomic determinants.

***Methods and Results*—**We used 3 experimental models: a polygenic model of cardiac hypertrophy and heart failure, a model of intrauterine growth restriction and *Lcn2*-knockout mouse; cultured cardiomyocytes; and 2 human cohorts: 114 type 2 diabetes mellitus patients and 2064 healthy subjects of the YFS (Young Finns Study). In hypertrophic heart rats, cardiac and circulating *Lcn2* was significantly overexpressed before, during, and after development of cardiac hypertrophy and heart failure. *Lcn2* expression was increased in hypertrophic hearts in a model of intrauterine growth restriction, whereas *Lcn2*-knockout mice had smaller hearts. In cultured cardiomyocytes, *Lcn2* activated molecular hypertrophic pathways and increased cell size, but reduced proliferation and cell numbers. Increased LCN2 was associated with cardiac hypertrophy and diastolic dysfunction in diabetes mellitus. In the YFS, *LCN2* expression was associated with body mass index and cardiac mass and with levels of inflammatory markers. The single-nucleotide polymorphism, rs13297295, located near *LCN2* defined a significant *cis*-eQTL for *LCN2* expression.

***Conclusions*—**Direct effects of LCN2 on cardiomyocyte size and number and the consistent associations in experimental and human analyses reveal a central role for LCN2 in the ontogeny of cardiac hypertrophy and heart failure. **(*J Am Heart Assoc*. 2017;6:e005971. DOI: 10.1161/JAHA.117.005971.)**

Key Words: concentric hypertrophy • C-reactive protein • gene coexpression networks • GlycA • hypertrophy • lipocalin-2 • NGAL • systems biology

From the School of Applied and Biomedical Sciences, Faculty of Science and Technology, Federation University Australia, Ballarat, Victoria, Australia (F.Z.M., P.R.P., S.A.B., I.R., Y.M., S.P.B., J. Kelly, F.J.C.); Heart Failure Research Group, Baker Heart and Diabetes Research Institute, Melbourne, Victoria, Australia (F.Z.M., M.I.); Centre for Systems Genomics (S.G.B., S.C.R., M.I.), School of BioSciences (S.G.B., M.I.), Department of Pathology (S.G.B., S.C.R., M.I.), Department of Microbiology and Immunology, Peter Doherty Institute (S.P.B.), and Department of Physiology (C.L.C., J.R.B., L.M.D., M.I., S.B.H., F.J.C.), The University of Melbourne, Victoria, Australia; Computational Medicine, Faculty of Medicine, University of Oulu and Biocenter Oulu, Oulu, Finland (P.W., A.J.K., P.S., M.A.-K., J. Kettunen); Department of Medicine, The University of Melbourne (S.K.P., B.W., P.M.S., M.E.W., L.M.B.) and Department of Cardiology (B.W., P.M.S., L.M.B.), Austin Health, Heidelberg, Victoria, Australia; NMR Metabolomics Laboratory, School of Pharmacy, University of Eastern Finland, Kuopio, Finland (P.S., M.A.-K., J. Kettunen); Research Centre of Applied and Preventive Cardiovascular Medicine, University of Turku, Finland (S.R., O.R.); Department of Clinical Physiology, University of Tampere and Tampere University Hospital, Tampere, Finland (M.K.); Fimlab Laboratories, Department of Clinical Chemistry, Pirkanmaa Hospital District, School of Medicine, University of Tampere, Finland (T.L., E.R.); National Institute for Health and Welfare, Helsinki, Finland (A.H., M.P., V.S., J. Kettunen); Institute for Molecular Medicine Finland, University of Helsinki, Finland (M.P.); Department of Clinical Physiology and Nuclear Medicine, Turku University Hospital, Turku, Finland (O.R.); Medical Research Council Integrative Epidemiology Unit (M.A.-K.) and School of Social and Community Medicine (M.A.-K.), University of Bristol, United Kingdom; School of Medicine, Deakin University, Waurn Ponds, Victoria, Australia (M.M., P.A.L.); Department of Cardiovascular Sciences, University of Leicester, United Kingdom (F.J.C.).

Accompanying Data S1, Tables S1 through S12, and Figures S1 through S4 are available at http://jaha.ahajournals.org/content/6/6/e005971/DC1/embed/inline-supplementary-material-1.pdf

*Dr Inouye, Dr Harrap, and Dr Charchar contributed equally to this work as co-senior authors.

Correspondence to: Fadi J. Charchar, PhD, University of Ballarat, Room 228, F Building, Oppy Drive, Mt Helen, Ballarat, Victoria 3350, Australia. E-mail: f.charchar@ballarat.edu.au

Received March 7, 2017; accepted May 2, 2017.

© 2017 The Authors. Published on behalf of the American Heart Association, Inc., by Wiley. This is an open access article under the terms of the Creative Commons Attribution-NonCommercial License, which permits use, distribution and reproduction in any medium, provided the original work is properly cited and is not used for commercial purposes.

Clinical Perspective

What is New?

- Using several animal models, in vitro and human studies, we identified *LCN2* as a central gene in the developmental origins of cardiac hypertrophy leading to heart failure.
- Increased LCN2 expression has defined effects of cardiomyocyte proliferation and hypertrophy that might explain cardiac hypertrophy and is likely to reflect chronic activation of inflammatory pathways.

What are the Clinical Implications?

- The experimental effects of LCN2 on cultured cardiomyocytes and in hearts of neonatal animals need to be corroborated in clinical studies of relationships between LCN2, heart size, and, if possible, cardiomyocyte numbers.
- LCN2 could be targeted as a therapeutic target and also developed as an early marker for cardiac hypertrophy and heart failure.

Cardiac hypertrophy is, after age, the single most important risk factor for cardiovascular death,[1] often as a result of heart failure. Hypertrophic remodeling of the heart is usually in response to increased workload, and the response to such stress has been shown to involve inflammatory pathways.[2–4] Indeed, chronic inflammatory processes have been implicated not only in response to stress, but also more generally as primary etiological factors in cardiovascular disease (CVD).[5] Cardiovascular remodeling depends on refashioning the interstitium, and inflammation stimulates molecules, such as matrix metalloproteinase-9 (MMP9), that degrade the interstitial matrix.[6] MMP9 levels have been associated with cardiovascular disease prognosis,[7] and MMP9 is stimulated by the protein lipocalin-2 (LCN2), also known as neutrophil gelatinase-associated lipocalin (NGAL).[8,9] LCN2 levels have been used to reflect tissue damage, particularly of the kidney, but more recently also for CVD manifestations,[10] including hypertensive cardiac hypertrophy,[11] coronary artery disease[12] and acute heart failure.[13] LCN2 has also been associated with long-term mortality following acute heart failure, independent of renal function.[14] However, it is unclear whether LCN2 is simply a marker of an inflammatory process or capable of direct effects on the heart that might contribute to cardiac hypertrophy and failure.

In this study, we investigated the association of LCN2 with concentric cardiac hypertrophy in genetic and environmental experimental models and in relation to the normal variation of human heart size and cardiac hypertrophy in diabetes mellitus. We examined transcriptional associations with LCN2 and identified genetic polymorphisms influencing *LCN2* expression. We determined the direct cellular effects of LCN2 in cultured cardiomyocytes. Our findings reveal increased LCN2 levels as a consistent association with cardiac hypertrophy in a variety of models and human cohorts, and our in vitro studies support a direct role for LCN2 in the origins of cardiomyocyte hypertrophy and reduced cardiomyocyte proliferation.

Methods

Detailed methods are available in the Data S1.

Genetic Model of Cardiac Hypertrophy and Heart Failure

The hypertrophic heart rat (HHR) is a normotensive inbred polygenic model of adult cardiac hypertrophy, heart failure, and premature death generated by us (Prof Stephen Harrap and Prof Lea Delbridge, University of Melbourne, Melbourne, Parkville, Australia).[15] HHRs have a reduced endowment of cardiomyocytes from very early life, a situation predisposing to hypertrophy and failure in later life.[15,16] Aged-matched male animals were sampled during the following periods: neonatal (postnatal day 2, n=11 HHR, n=10 Normal Heart Rat [NHR]), adolescent (4 weeks old, n=4 HHR and n=4 NHR for cardiomyocyte isolation), young adult (13 weeks old, n=7 HHR, n=7 NHR; 35 weeks old, n=8 NHR, n=11 HHR), and old adult (50 weeks old, n=11 HHR, n=10 NHR).

Animals were euthanized by decapitation (neonatal) or with an overdose of pentobarbitone (Lethobarb; adult animals). The heart was immediately removed, and ventricles were dissected from the atria. Cardiac weight index (mg/g) was calculated from the total heart weight (mg) relative to total body weight (g) of the animal. The studies involving animals were approved by the Animal Ethics Committee of Deakin University and the University of Melbourne and ratified at Federation University Australia. They were performed according to the "Code of Practice for the Care and Use of Animals for Scientific Purposes" from the National Health & Medical Research Council of Australia.

Rat Microarray Experiments

RNA was extracted from the left ventricle of 2-day-old HHRs and NHRs (n=8/group, no pooling), and Affymetrix GeneChip Rat Gene 1.0 ST Arrays (Affymetrix, Santa Clara, CA) was used to assess genes differentially expressed with the assistance of the Ramaciotti Centre for Gene Function Analysis. The data set obtained has been deposited in the National Center for Biotechnology Information Gene Expression Omnibus

database according to Minimum Information About a Microarray Experiment guidelines with series accession number GSE38607. Differentially expressed genes were identified using a 2-sample *t* test in the Partek Genomics Suite (version 6.6; Partek Inc, Chesterfield, MO), with Bonferroni-adjusted $P<0.05$ and fold difference higher than 2.

Lcn2 mRNA and Protein Levels in Models of Cardiac Hypertrophy and Heart Failure

Primers and conditions used for all real-time quantitative PCR (qPCR) are shown in Table S1. Amplification reactions used the SensiFast SYBR Low-ROX Kit qPCR reagent system (Bioline Reagents Ltd, London, UK) in a Viia7 qPCR instrument (Life Technologies, Life Technologies, Carlsbad, CA). Immunohistochemistry was performed using an anti-LCN2 Rabbit Polyclonal antibody (1:200 dilution, TA322583; OriGene Technologies, Rockville, MD), followed by the EnVision+System-HRP. Western blots were performed as previously described[17] using anti-LCN2 Rabbit Polyclonal antibody or β-actin (Cell Signaling Tecnology, Danvers, MA). Lcn2 plasma and left ventricle (LV) protein levels were measured by ELISA in duplicates in neonatal and adult HHR and NHR using the Lipocalin-2 Rat ELISA Kit (Abcam, Cambridge, UK) according to the supplier. Sanger sequencing was used to sequence 10 000 base pairs (bp) before and 2000 bp after the Lcn2 gene in the HHR and NHR (Table S1).

Lcn2-Knockout

Whole body and heart size of adult (12- to 13-week-old) Lcn2-KO (n=6) and age-matched wild-type mice C57BL/6 (n=4), generously donated by Prof Alan Aderem (Institute for Systems Biology, University of Washington, Seattle, WA), were measured upon death, and cardiac weight index was calculated as described above.

Intrauterine Growth Restriction Rat Model

An environmental model of cardiac hypertrophy was developed using Wistar Kyoto rats by intrauterine growth restriction, induced by uteroplacental insufficiency on day 18 of pregnancy (term being 22 days), was also investigated.[18,19] Six-month-old operated female and male rats (n=9) were compared to Wistar Kyoto female and male sham rats (n=16).

In Vitro Experiments

The pExpress vector containing the cDNA for the rat Lcn2 (2 ng/mL, MRN1768-98079404; Thermo Fisher Scientific, Waltham, MA) or empty vector (pExpress) were transfected into rat embryonic ventricular myocardial cells (H9c2) using Lipofectamine 2000 (Life Technologies). We counted the number of cells by hemocytometry with the use of the Countess Automated Cell Counter (Life Technologies). Wheat germ agglutinin and Hoechst staining was used to measure cell size,[20] and phospho-histone H3 staining was used to determine cell proliferation.[20] Apoptosis was investigated by flow cytometry using an Annexin-V: FITC Apoptosis Detection Kit I. All in vitro experiments were independently repeated 3 times, each time in triplicates.

RNA-Sequencing and Molecular Pathways

RNA was extracted from Lcn2-KO mice and cells transfected with Lcn2 plasmid for 48 hours (and respective controls). RNA from 3 samples of each group was sent to RNA-sequencing at the Australian Genome Research Facility using the Illumina HiSeq platform (v3 chemistry 100 bp paired-end sequencing). Each sample was considered an individual sample and no pooling was performed. Analysis of differential expression was performed in the R statistical programming environment (version 3.1.0) using Rsubread (version 1.14.2) and edgeR (version 3.6.8) Bioconductor packages (Table S2).[21] *P* values were adjusted for multiple testing using the Benjamini-Hochberg correction with a false discovery rate <0.05. Gene ontology enrichment analysis was performed on filtered lists of differentially expressed genes to ask which pathways were enriched in genes differentially expressed.

Human Echocardiography Measurements

Briefly, 114 individuals with echocardiographic measures were selected from a prospective cohort of type 2 diabetic subjects[22] whose basic characteristics are shown in Table S3. In addition, subjects with echocardiographic measures from the Young Finns Study (YFS) analyzed, shown in Table S4. The YFS is a longitudinal population-based study of 3596 individuals recruited during childhood in 1980.[23] Genome-wide genotype data, transcriptome-wide microarray profiling, C-reactive protein (CRP), glycoprotein acetylation (GlycA), and echocardiographic measurements were available for different subsets of 2064 individuals aged 34 to 48 years, participating in the 2011 follow-up study.[24–27] The cohort studies complied with the Declaration of Helsinki and were approved by the human ethics committee at each institution. All subjects gave informed consent.

In both cohorts, echocardiographic examinations were performed using transthoracic echocardiography by an Acuson Sequoia 512 (Acuson, Mountain View, CA) with a 3.5-MHz scanning frequency phased-array transducer. From the ultrasound images, LV structure, systolic, and diastolic function were measured following the guidelines of the American Society of Echocardiography, as previously described.[28,29]

Cardiac hypertrophy was defined as LV mass indexed to the body surface of >95 g/m^2 in women and >115 g/m^2 in men.[30] E/E′-ratio was calculated using the average values of lateral and septal e′ velocity.[29]

Human Plasma LCN2 Measurement

Human plasma was used to measure LCN2 levels in duplicates in 121 subjects with type 2 diabetes mellitus using the Quantikine ELISA Human Lipocalin-2 Immunoassay (R&D Systems, Minneapolis, MN), according to the supplier.

LCN2 mRNA Levels in Human Heart

We used data in the repository Gene Expression Omnibus series GSE1145 to investigate the levels of LCN2 in human idiopathic dilated hearts (n=11 control hearts and n=15 idiopathic dilated hearts). We performed a whole-genome analysis using the Gene Expression Omnibus tools, including false discovery rate <0.05, to determine whether LCN2 was overexpressed in human idiopathic dilated hearts.

GlycA Measurement

GlycA reflects the integrated concentrations and glycosylation states of several of the most abundant inflammatory acute-phase glycoproteins[31,32] measured with a proton nuclear magnetic resonance metabolomics platform.[33]

CRP Measurement

High-sensitivity CRP was quantified from serum samples using an automated analyzer with a latex turbidimetric immunoassay kit.

Coexpression Networks and Quantitative Trait Loci

Transcriptome-wide microarray profiling was performed on whole blood for 1650 individuals in the YFS as previously described.[24] Briefly, stabilized total RNA was obtained from whole blood for individuals in the YFS. RNA was hybridized to Illumina HT-12 (version 4; Illumina, San Diego, CA) BeadChip arrays, and raw probe data were exported with the Illumina BeadStudio software. Both positive and negative control probes were used to quantile normalize using the *limma* R package.[34] Probe intensities were reported on a $\log_2$ scale.

Identification and characterization of the gene coexpression network analyzed in this study is described in Ritchie et al.[32] Here, we defined the neutrophil module's coexpression as the Spearman's correlation coefficient between its 27 genes.[32] The average expression was used for genes with multiple microarray probes. Edges in the coexpression network were defined as the magnitude of the correlation exponentiated to the power of 4. A vector summarizing module expression was calculated for association testing as the first eigenvector of a principal components analysis on module expression. This summary expression profile captured 57% of the total variation in module gene expression. Association analyses are described in the Statistical Analyses section below.

Genome-wide genotyping was carried out on whole-blood samples for 2442 individuals participating in the 2001 follow-up study of the YFS as previously described.[25] Sample and genotype quality control was performed for these 2442 individuals (Data S1). A combined total of 6 721 082 directly genotyped and imputed single-nucleotide polymorphisms (SNPs) passed quality control.

Module quantitative trait loci (QTLs) were identified for 1386 individuals with matched genotype and gene expression data in the YFS through a genome-wide scan for SNPs associated with the summary expression profile using PLINK 1.90 beta (version 3.32). Individual associations were tested using a linear model of minor allele dosage on neutrophil module summary expression. An SNP was considered a module QTL where $P<5\times10^{-8}$ (genome-wide significance). Models were adjusted for age, sex, and the first 2 principal components of the genotype data. The module QTL, rs13297295, on chromosome 9 was further tested for an association with *LCN2* expression levels using the same model. Rs13297295 was also tested for association with GlycA and CRP in the 1712 individuals with matched genotype and GlycA or CRP data.

Statistical Analyses

R software (version 3.13; R Foundation for Statistical Computing, Vienna, Austria) was used for the analyses of the YFS data. The *NetRep* package (version 0.54) was used for network analyses.[35] Measurements of GlycA, routine lipids, CRP, body mass index (BMI), heart function (measured as early filling [E] to early diastolic mitral annular velocity [E′]—E/E′ ratio, and E to late [A] diastolic filling—E/A ratio) were normalized using a natural logarithm transformation, and all continuous measurements were standardized to SD units in both cohorts. Module associations with the inflammatory biomarkers were assessed by linear regression of: neutrophil module expression on GlycA and CRP; linear regression of *LCN2* expression on GlycA and CRP. To assess whether *LCN2* was a mediator of the relationship between these biomarkers and the neutrophil module, we used linear regression of: GlycA and CRP on LCN2 expression and neutrophil module expression; CRP on LCN2 expression and neutrophil module expression; and GlycA on LCN2 expression and neutrophil module expression. All terms in the models were additive, and all models were adjusted for age and sex. Matched gene expression, GlycA, and CRP data

were available for 1650 individuals. Associations between *LCN2* expression and echocardiographic measurements in the YFS (Table S5) were tested by linear regression of each echocardiographic measurement on *LCN2* expression, adjusting for age and sex. Each association was considered significant where $P<0.05$. Matched gene expression and echocardiographic data were available for between 1482 and 1573 individuals depending on the LV phenotype.

Inter- and intraassay coefficients of variability were calculated for ELISAs, and only less than 15% variability was accepted (hence 7 human samples from the type 2 diabetes mellitus cohort were excluded from further analyses). Human plasma LCN2 levels were not normally distributed; therefore, LCN2 was log transformed for the association analyses presented in Table S3. An independent *t* test was used to assess differences in continuous variables between those with and without cardiac hypertrophy or chi-square analyses for dichotomous variables. A general linear model analysis was performed to test for associations between presence of cardiac hypertrophy and plasma LCN2 levels after adjusting for variables from the univariable analysis with a *P* value of <1.0 (age, sex, BMI, estimated glomerular filtration rate, and systolic blood pressure). We used untransformed LCN2 levels to perform Spearman Rho correlations between human plasma LCN2 and LV left ventricle mass and function in the type 2 diabetes mellitus cohort (Table S6). Significance was set at $P<0.05$.

Results from the animal groups were tested for normal distribution using the Skewness and Kurtosis tests. Independent sample *t* tests (with Welch's correction in the case of different variance) and ANOVA were used to compare the data between the animal groups. A 2-way ANOVA was used to compare between Lcn2 expression in the different cell types in HHRs and NHRs.

Results

Lcn2 Is Associated With Cardiac Size in Experimental Genetic and Environmental Models

HHR and NHR

A transcriptome analysis of neonatal P2 LV tissue identified 21 genes with significant differential expression between HHRs and NHRs (Table S7 and Figure S1) involving pathways for cardiovascular system development and function, and cell growth and proliferation (Tables S8 and S9), with *Lcn2* showing the greatest differential expression ($q=7\times10^{-11}$; Table S7). Elevated cardiac Lcn2 expression was validated by qPCR at postnatal day 2 (Figure 1A) and was found to persist with established hypertrophy at 13 weeks of age and with the emergence of heart failure at 35 or 50 weeks of age (Figure 1B) and further confirmed by 25-kDa Lcn2 monomer protein analyses (Figure 1C and 1D). Compared with its control strain, the NHR, we found significantly higher circulating Lcn2 in adult HHRs with established hypertrophy at 35 weeks of age (Figure 1E), but also soon after birth (Figure 1F) before hypertrophy is evident but cardiomyocyte numbers are already reduced. RNA and immunohistochemical studies (Figure 1G and 1H) showed Lcn2 expression in cardiomyocytes and noncardiomyocyte (fibroendothelial) cells. Correlation between cardiac *Lcn2* mRNA and plasma Lcn2 in the HHRs and NHRs was $r=0.996$ ($P<0.001$).

Sequencing the HHR and NHR *Lcn2* genes for comparison with the published sequence for spontaneously hypertensive rats and Fisher 344 (original progenitors of HHR and NHR), we found 3 unique SNPs in the HHR, all inherited from the spontaneously hypertensive rats, with 1 being intronic and 2 being upstream of the coding sequence (Figure 2A through 2D). In the HHR heart, both *Lcn2* mRNA and pre-mRNA levels were increased (Figure 2E), suggesting a transcriptional dysregulation of *Lcn2* in the HHR. Transcription Factor Affinity Prediction (sTRAP)[36,37] analysis suggested that one of these SNPs (rs196968512) created a binding site for the enhancer, RAR-related orphan receptor A (Figure 2B and 2F).[38]

Lcn2 knockout mice

Hearts from adult mice with double knockout of the *Lcn2* gene (Lcn2-KO)[39] were significantly smaller than age-matched wild-type mice (cardiac weight index 5.4 versus 5.9 mg/g; $P=0.03$; Figure 3A). RNA-sequencing of murine heart tissue from *Lcn2*-KO versus wild-type identified 16 significantly differentially expressed genes (Table S10) that are relevant to pathways related to hypertrophic cardiomyopathies (Table S11; Figure 3B and 3C).

Intrauterine growth restricted rats

Last, in an environmental model of intrauterine growth restriction,[18,19] we demonstrated that subsequent adult cardiac hypertrophy was associated with significantly higher levels of cardiac *Lcn2* mRNA ($P=0.0214$; Figure 4).

Lcn2 Overexpression Induces Hypertrophy in Cardiomyocytes and reduces proliferation

We next sought to determine whether increased *Lcn2* transcription in cardiomyocytes results in a hypertrophic phenotype. We transfected rat embryonic ventricular myocardial cells with a plasmid containing the *Lcn2* mRNA sequence and performed imaging and RNA-sequencing analyses. Significant increase in the expression of *Lcn2* in transfected cells (log fold change=4.44; $q=0.0005$; Figure S2) resulted in a significant increase in the size of transfected cells (Figure 5A and Figure S3A). In these hypertrophic cells, we found significantly increased expression of 2 genes previously linked

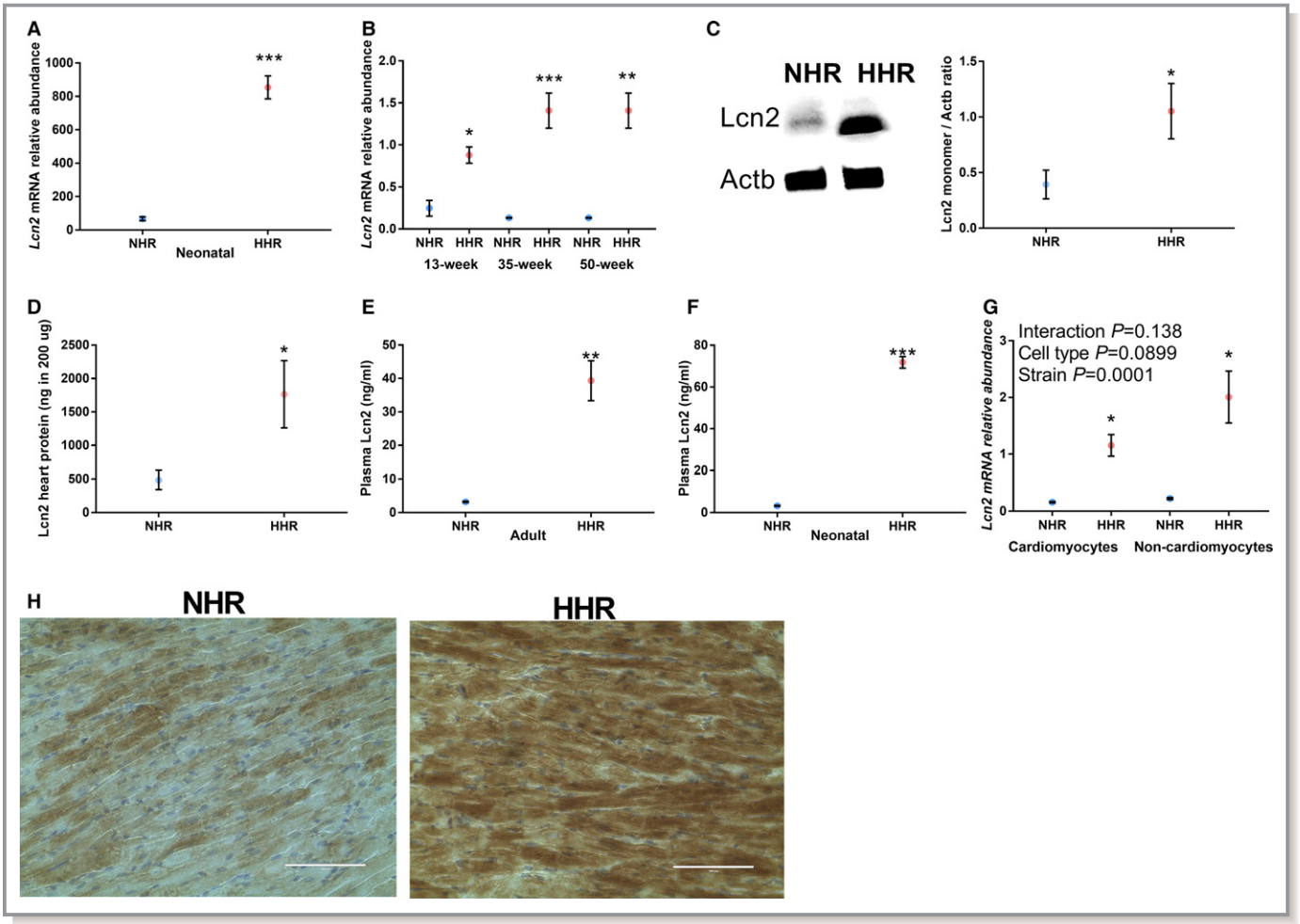

Figure 1. Overexpression of lipocalin-2 (*Lcn2*) in a polygenic model of cardiac hypertrophy. A, Relative expression levels of *Lcn2* mRNA measured by real-time PCR in the heart of 2-day-old hypertrophic heart rat (HHR; n=10) compared to normal heart rat (NHR; n=8; $P<0.0001$), (B) 13-week-old ($P=0.016$; n=9/strain), 35-week-old ($P<0.001$; n=8 NHR and n=11 HHR), and 50-week old ($P=0.0015$; n=8 NHR and n=11 HHR) HHR compared to NHR. Heart Lcn2 (25-kDa monomer) protein is significantly higher in the HHR compared with NHR, measured by both (C) western blot ($P=0.039$; n=3/strain) and (D) ELISA ($P=0.029$; n=4/strain). E, Rat plasma Lcn2 in 35-week-old ($P=0.0009$; n=6/strain) and (F) 2-day-old ($P<0.0001$; n=5/strain) HHR compared to NHR. G, *Lcn2* mRNA in cardiomyocytes ($P=0.013$; n=4/strain) and noncardiomyocytes ($P=0.03$) in the NHR and HHR. The interaction explained 5.135% of total variation ($P=0.138$), the cell type 6.91% of variation ($P=0.0899$), and the strain explained the majority of variation (63.58%; $P=0.0001$). H, Lcn2 staining in NHR and HHR hearts (×400 magnification; scale bar=200μm). *$P<0.05$; **$P<0.01$; ***$P<0.001$. Data shown as mean and error bars represent SEM.

with hypertrophic cardiomyopathy—thrombospondin 2 (log fold change=−0.36; q=0.0005) and dynamin 1 (log fold change=−0.48; q=0.044).[40,41] In addition to hypertrophy, overexpression of *Lcn2* resulted in a significant decrease in cell numbers (Figure 5B) with a concomitant reduction in cells positive for phosphorylated histone H3, reflecting reduced cell mitosis (Figure 5C and Figure S3B). No change in apoptosis was observed (Figure S4). Pathway enrichment analysis of the 529 genes with nominally significant evidence of differential expression (unadjusted $P<0.05$) between transfected and control myocytes suggested dysregulation of genes related to cell cycle (Kyoto Encyclopedia of Genes and Genomes rno04110; $P=0.006$). There was suggestive evidence for genes related to hypertrophic cardiomyopathy (Kyoto Encyclopedia of Genes and Genomes rno05410; $P=0.07$) and dilated cardiomyopathy (Kyoto Encyclopedia of Genes and Genomes rno05414; $P=0.09$; Figure 5D and 5E; Table S12).

Human LCN2 Is Associated With LV Hypertrophy in Diabetes Mellitus

Obesity and type 2 diabetes mellitus have been associated with elevated levels of plasma LCN2.[42,43] Independently from those findings, cardiac hypertrophy has been associated with diastolic dysfunction and is recognized as a diabetic complication.[44] However, whether cardiac hypertrophy and diastolic dysfunction in type 2 diabetic patients is associated with high

A

Ensembl SNP ID	Position in Chr 3 (Mb)	Gene, region	Reference*	F344*	SHR*	HHR	NHR
N/A	16,761,925	Non-coding	T	A	T	T	T
N/A	16,762,516	Non-coding	G	A	G	G	A
rs105835971	16,762,818	Non-coding	C	T	C	C	T
rs107576696	16,763,461	*Lcn2*, intron	A	G	A	A	G
rs105932663	16,763,468	*Lcn2*, intron	A	G	A	A	G
rs198262931	16,763,494	*Lcn2*, intron	C	C	T	T	C
rs106590638	16,763,641	*Lcn2*, intron	A	G	A	A	G
N/A	16,764,279	*Lcn2*, exon	G	A	G	G	A
rs107418419	16,765,330	*Lcn2*, intron	G	A	G	G	A
N/A	16,767,449	Non-coding	C	T	C	C	T
rs196968512	16,767,791	Non-coding	C	C	T	T	C
rs197438455	16,769,206	Non-coding	G	G	T	T	T
rs198863472	16,769,310	Non-coding	T	C	C	C	C
rs198754687	16,769,518	Non-coding	C	C	T	T	C
rs197694599	16,769,973	Non-coding	T	C	C	C	C

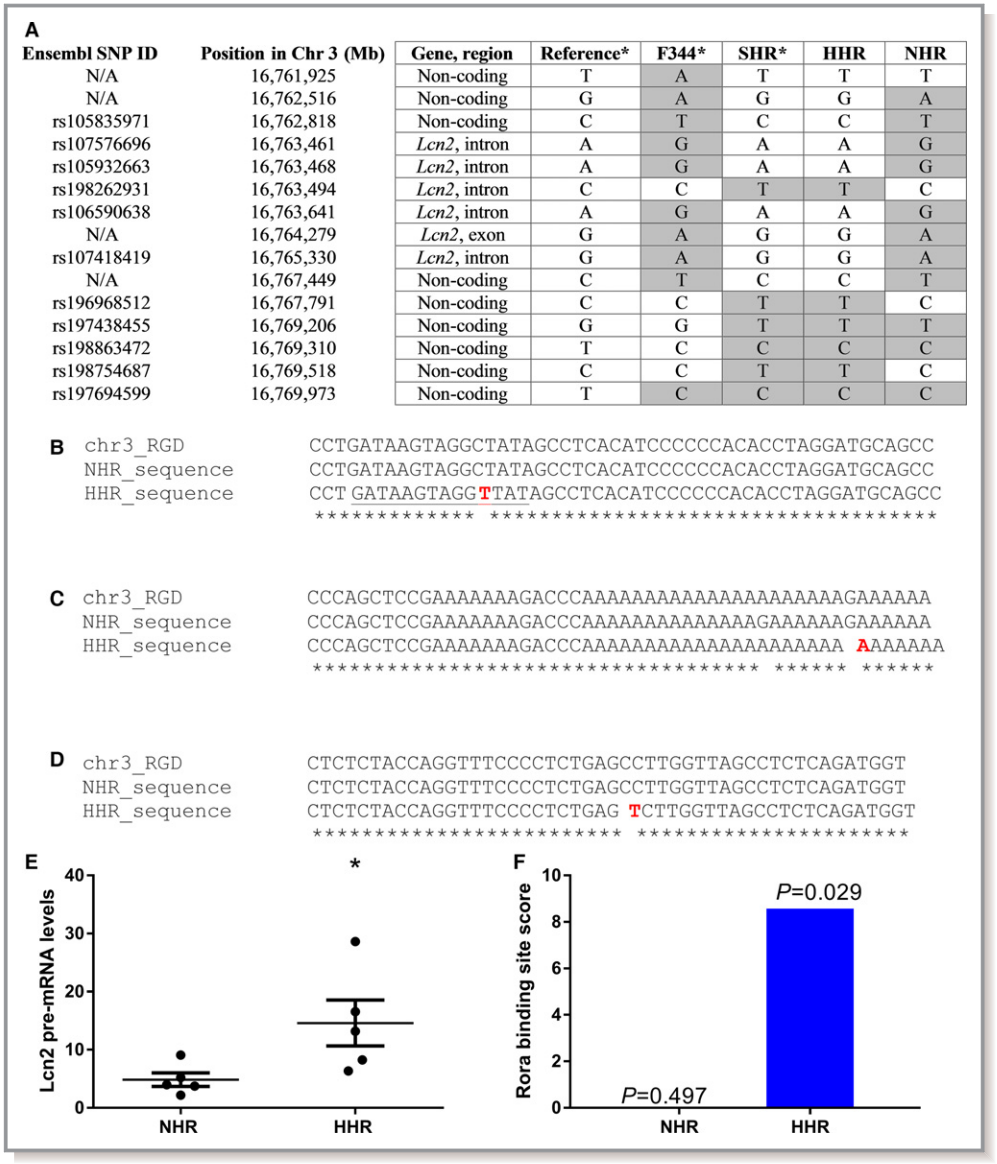

Figure 2. Variants in the lipocalin-2 (*Lcn2*) gene, showing regions with variants in the HHR, according to the Rat Genome Database (RGD; version 5). A, Genotype analysis of the region of 10 000 bp around the *Lcn2* gene, showing the origin of the variants observed in the HHR. Highlighted in gray are variants that differ from the reference genome, showing that the HHR carries 3 unique variants which were inherited from the SHR. B, Single-nucleotide polymorphism (SNP) on chr3: 16 767 791 (rs196968512 C/T) 1401 bp upstream of Lcn2 gene. C, SNP on chr3: 16 767 398 (G/A) in a highly conserved region 1001 bp upstream the Lcn2 gene. D, Nonfunctional intronic SNP originally from SHR on position chr3: 16 763 494 (rs198262931 C/T). E, *Lcn2* pre-mRNA is also upregulated in the HHR compared to the NHR (n=5/strain), suggesting that it is dysregulated at the transcriptional level. F, The SNP, rs196968512, creates a new binding site for the transcription factor, Rora (region underlined in B), which acts as an enhancer for expression of *Lcn2* and is exclusive of the HHR. The figure shows the binding site score and the *P* values for the binding of Rora to that region. chr3 indicates rat chromosome 3; F344, Fisher 344 rat; HHR, hypertrophic heart rat; N/A, nonannotated SNP; NHR, normal heart rat; RGD, reference sequence from the Rat Genome Database v5; SHR, spontaneously hypertensive rat.

LCN2 levels is not known. Echocardiographic assessment of 114 patients with type 2 diabetes mellitus and normal renal function revealed significantly higher levels of mean plasma LCN2 in the 30 diabetic subjects with LV hypertrophy than those 84 without 44.0 ng/mL [95% CI, 38.3−50.6] versus 36.0 ng/mL [33.1−39.2] *P*=0.017) that remained after adjustment for age, sex, BMI, estimated glomerular filtration rate, and systolic blood pressure (*P*=0.034; Figure 6A). There

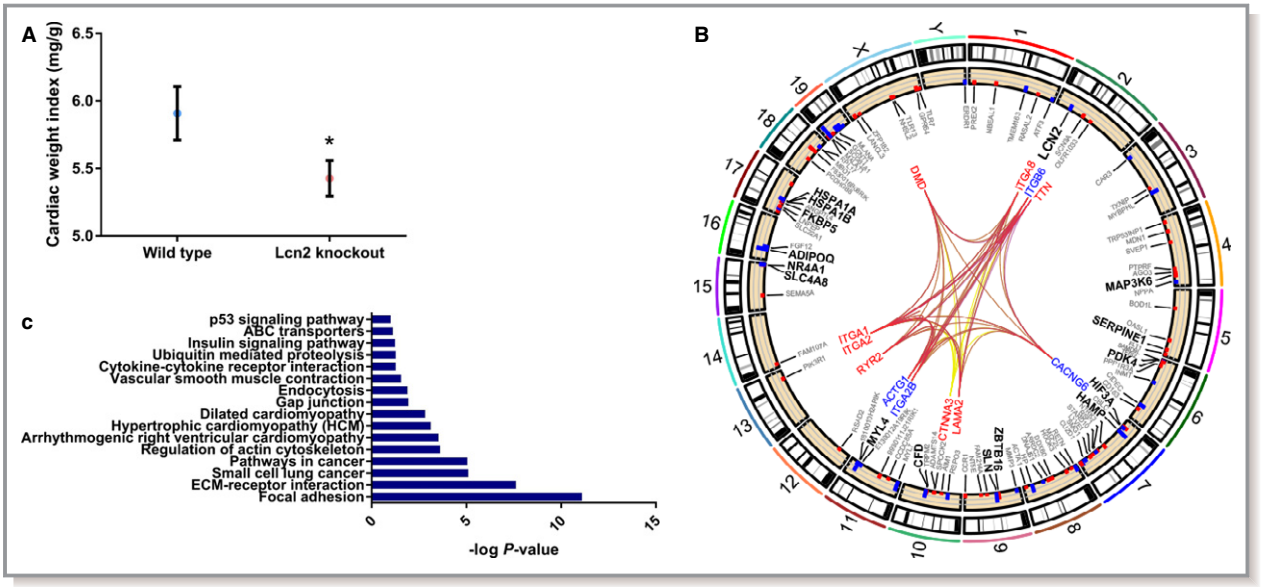

Figure 3. Heart size and associated pathways in lipocalin-2 (Lcn2)-knockout (KO) mice. A, Adult Lcn2-knockout mice have smaller hearts (*P=0.033; n=4 wild-type and n=6 Lcn2 KO). Data shown as mean and error bars represent standard error of mean. B, Genes and pathways differentially regulated in the heart of Lcn2-knockout. Hypertrophic cardiomyopathy (KEGG mmu05410, P=0.0007) is shown in red, dilated cardiomyopathy in blue (Kyoto Encyclopedia of Genes and Genomes [KEGG] mmu05412; P=0.008) and arrhythmogenic right ventricular cardiomyopathy in yellow (KEGG mmu05412; P=0.0003). The genes of dilated cardiomyopathy and hypertrophic cardiomyopathy pathways were the same, and therefore lines are overlapped. Each edge point indicates the chromosomal location for genes identified in specific pathways from the differentially expressed genes. Bar plots are the differentially expressed genes in each pathway. Red depicts genes upregulated, and blue those downregulated, represented as log2 fold change. C, Gene ontology analysis, showing −log P value. ABC indicates ATP-binding cassette; ECM extracellular matrix.

was a positive correlation between LCN2 levels and LV mass (n=114; Spearman's r=0.22; P=0.018; Figure 6B and Table S6). In diabetic subjects with cardiac hypertrophy, there was evidence of diastolic dysfunction (Table S3) with a significantly increased E/E′ ratio (mean±SD 15.2±4.5 versus 11.4±3.5; P<0.0001), but there was no association between these measurements and LCN2 (Table S6).

LCN2 mRNA Is the Human Heart

From subjects with idiopathic dilated cardiomyopathy, cardiac RNA expression data in a public repository (GSE1145) revealed overexpression of cardiac *LCN2* after adjustment for multiple comparisons (Figure 6C; false discovery rate, q=0.008).

LCN2 Expression, Cardiac Size and Function, and BMI in the YFS

In the 1590 YFS individuals (mean age, 42 years) with matched echocardiographic and whole-blood gene expression data, linear regression analysis adjusted for age and sex showed that *LCN2* expression was associated with various structural and functional LV phenotypes (Table S5). Higher *LCN2* expression was associated with increased heart rate ($P=6\times10^{-6}$), LV end-diastolic volume (P=0.02), and cardiac output ($P=3\times10^{-6}$). LV mass ($P=5\times10^{-5}$) and thickness of the interventricular septum ($P=8\times10^{-4}$) were also positively correlated with *LCN2* expression. Although the negative correlation between *LCN2* expression and E/A ratio ($P=5\times10^{-4}$) suggested diastolic impairment, this might have been confounded by the increased heart rate,[45] given that other measures of diastolic function (E/E′ ratio, mitral E-wave declaration time, and isovolumic relaxation time) did not show significant

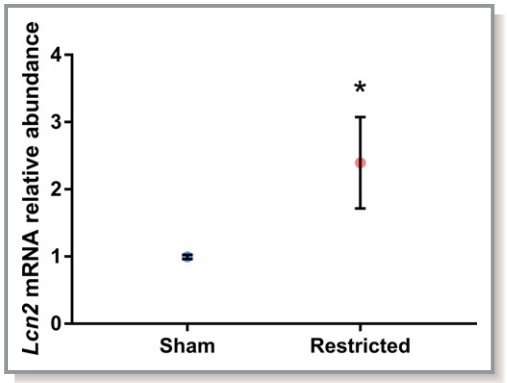

Figure 4. Environmental model of cardiac hypertrophy overexpresses lipocalin-2 (*Lcn2*) mRNA (*P=0.0214; n=16 sham and 9 restricted mice). Data shown as mean and error bars represent SEM.

correlations with *LCN2* expression (Table S5). There was also no significant correlation between *LCN2* expression and indices of systolic function, including ejection fraction and systolic wall velocities (Table S5). In addition, *LCN2* expression correlated significantly with BMI (r=0.33; 95% CI, 0.28–0.37; $P=8\times10^{-42}$). In terms of LV phenotypes, BMI was associated with increased LV size, heart rate, end-diastolic volume, and cardiac output (data not shown). There was also more consistent evidence of reduced diastolic function with increasing BMI, although systolic function was normal. Regression models that included *LCN2* expression and BMI revealed that the correlation between BMI and *LCN2* expression could account for the associations observed for *LCN2* expression alone (data not shown). This has been reported previously and interpreted as part of the low-grade inflammatory activation that accompanies obesity and predisposes to insulin resistance and type 2 diabetes mellitus.[42]

LCN2 Is Central to a Neutrophil Gene Coexpression Network and Is Under Genetic Control

Previous analysis of whole-blood gene expression data identified a reproducible tightly coexpressed gene module

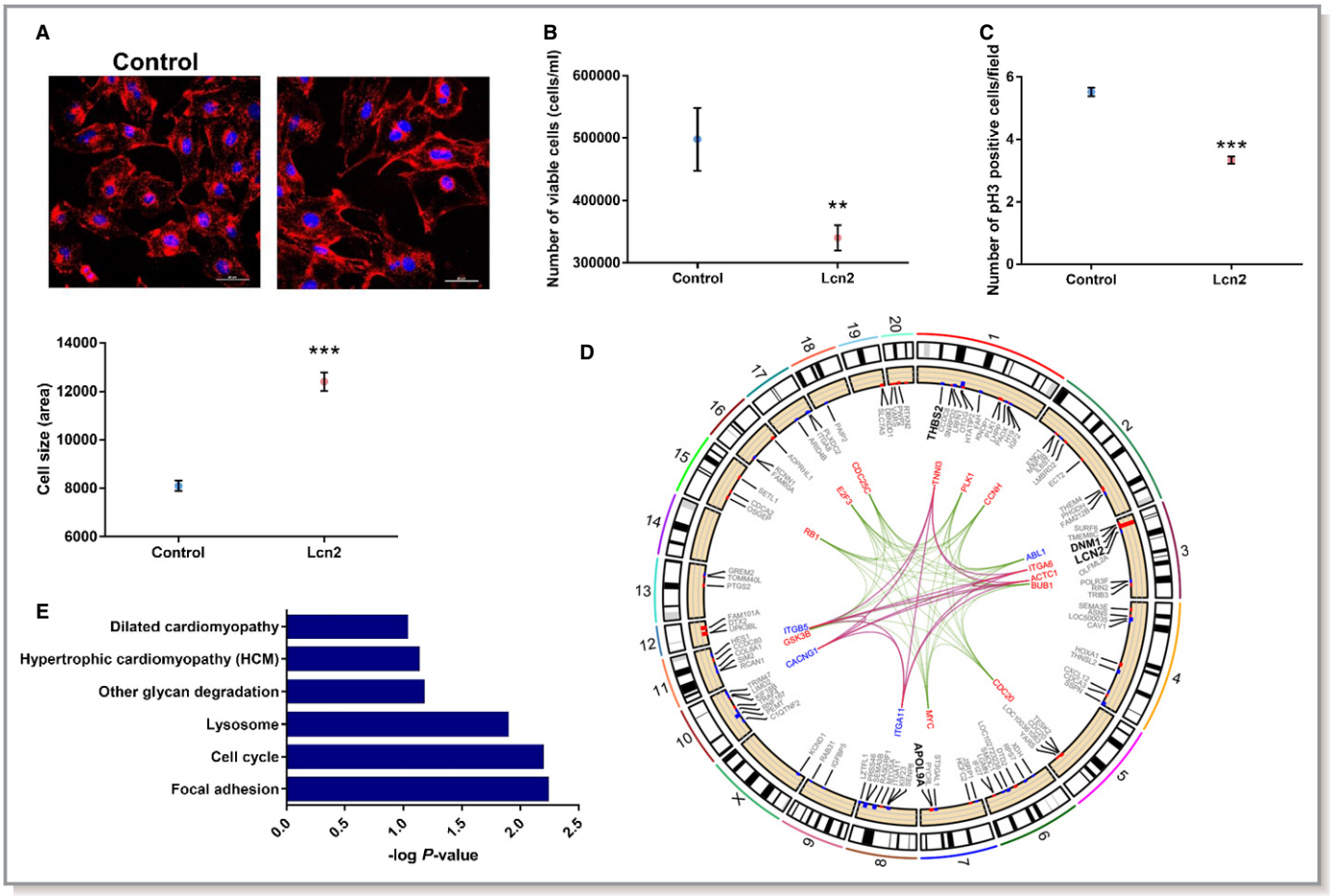

Figure 5. Role of lipocalin-2 (*Lcn2*) in cardiac cells. A, Representation of wheat-germ agglutinin (red) and DAPI (blue) staining, used to estimate cell size (×400 magnification; scale bar=60 μm). Overexpression of Lcn2 increased the size of the cells when compared with cells transfected with the empty plasmid (P<0.0001). B, Overexpression of Lcn2 reduced the number of cells measured by hemocytometer (P=0.0052). C, Overexpression of Lcn2 resulted in cell-cycle arrest, observed by reduced phosphorylation of histone H3 (pH3; ×200 magnification; scale bar=100 μm; P<0.0001). D, Genes and pathways differentially regulated with overexpression of Lcn2. Cell cycle (Kyoto Encyclopedia of Genes and Genomes [KEGG] rno04110; P=0.006) is shown in green, hypertrophic cardiomyopathy (KEGG rno05410, P=0.07) in red, and dilated cardiomyopathy (KEGG rno05414; P=0.09) in blue. Genes of dilated cardiomyopathy and hypertrophic cardiomyopathy pathways were the same, and therefore lines overlapped. Each edge point indicates the chromosomal location for genes identified in specific pathways from the differentially expressed genes. Bar plots are the differentially expressed genes in each pathway. Red depicts genes upregulated, and blue those downregulated, represented as log2 fold change. E, Gene ontology analysis, showing −log P value. All experiments were run in 3 independent experiments, with at least 3 replicates each (total, 9 replicates). For experiments involving confocal microscopy, 10 different fields were analyzed per replicate. Positive controls were added to all experiments. **P<0.01; ***P<0.001. Data shown as mean and error bars represent SEM.

associated with elevated levels of inflammatory markers in 2 independent healthy population studies.[32] This module was significantly enriched for genes involved in the innate immune response, in particular neutrophil function.[32] Among these, the expression of *LCN2* showed high centrality to the neutrophil module (Figure 7), with a scaled connectivity (Data S1) of 0.65 and a correlation of 0.89 with the module's summary expression profile. In a healthy population of 1650 individuals from the YFS cohort (Table S4), we found that the module summary expression was independently associated with both GlycA (β=0.16; 95% CI, 0.11–0.21; $P=2\times10^{-9}$) and CRP (β=0.15; 95% CI, 0.093–0.20; $P=5\times10^{-8}$) when both were included in the same model, suggesting the module is related to inflammatory processes reflected by both biomarkers. Although *LCN2* expression itself was independently associated with both GlycA (β=0.18; 95% CI, 0.12–0.23; $P=7\times10^{-11}$) and CRP (β=0.19; 95% CI, 0.14–0.24; $P=3\times10^{-12}$), GlycA and CRP were no longer significant when *LCN2* was included in the model. This suggests that *LCN2* on its own is a better predictor of the module summary profile. To determine the potential genetic determinants of the neutrophil module function, we performed a QTL scan on the neutrophil module's summary expression (Data S1) in 1650 healthy individuals from the YFS cohort. We found that rs13297295, the top module QTL, was located 750 kb downstream from *LCN2* to which it was a *cis*-eQTL, with each "C" allele at rs13297295 increasing expression of *LCN2* by 0.39 SD ($P=2\times10^{-9}$; adjusted for age, sex, and 2 genetic principal components). There was no detectable association between rs13297295 and CRP or GlycA. Taken together, these results suggest that increased *LCN2* expression is central to the inflammatory gene module.

Discussion

Our experimental and human studies reveal increased levels of LCN2 as a consistent correlate of cardiac hypertrophy (summarized in Figure 8). This relationship existed in the HHR polygenic model of spontaneous cardiac hypertrophy leading to heart failure, in Lcn2 gene knockout mice, but also in an environmental model of cardiac hypertrophy following intrauterine growth retardation. In human studies, LCN2 was associated with cardiac hypertrophy in healthy subjects of the YFS and in patients with type 2 diabetes mellitus. Importantly, our in vitro studies of *Lcn2* overexpression showed that it can activate hypertrophic pathways and cause an increase in cardiomyocyte size but a decrease in their proliferation. Irrespective of the primary cause of increased LCN2, these direct cellular effects provide a common fundamental pathophysiology for the contribution of LCN2 to cardiac hypertrophy.

This is the first time that a specific cardiomyocyte hypertrophic effect of LCN2 has been demonstrated. Previous studies have focused on the effects of LCN2 on the interstitial matrix through induction of the proteinase, MMP9. This is relevant to the degradation of intercellular matrix as part of the remodeling of the heart during the development of hypertrophy. However, we could find no significant variation in MMP9 expression in association with changes in *Lcn2* in HHR and *Lcn2* knockout mice (data not shown). It would also be beneficial to submit *Lcn2* knockout mice to stressors such as transverse aortic constriction to further understand the role of *Lcn2* in heart disease, but this was outside the scope of this study.

Interestingly, we observed that *Lcn2* expression reduced in vitro cardiomyocyte proliferation and cell numbers. It might seem counterintuitive that a limitation of cardiomyocyte

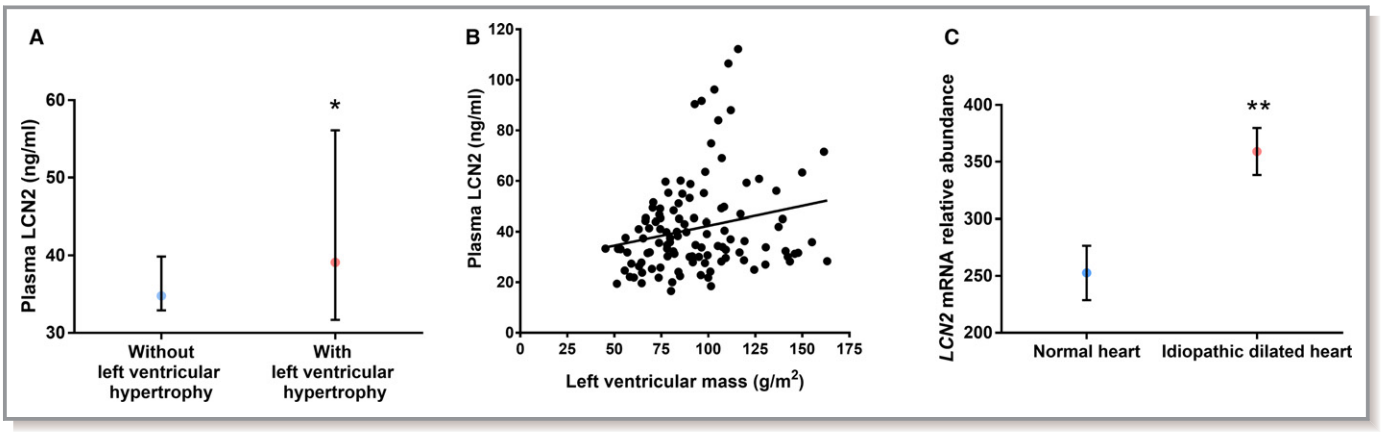

Figure 6. Lipocalin-2 (LCN2) is associated with human cardiac hypertrophy. A, Plasma levels of LCN2 were higher in patients with echocardiographically determined left ventricular hypertrophy (n=30) compared with those without (n=84; *P*=0.017, showing the median and 95% CI). B, There was a positive correlation between LCN2 levels and left ventricular mass (n=114; Spearman's *r*=0.22; *P*=0.018). C, LCN2 was overexpressed in human idiopathic dilated hearts compared with normal hearts (*P*=0.008 after adjustment for false discovery rate). Data shown as mean and error bars represent SEM. **P*<0.05; ***P*<0.01.

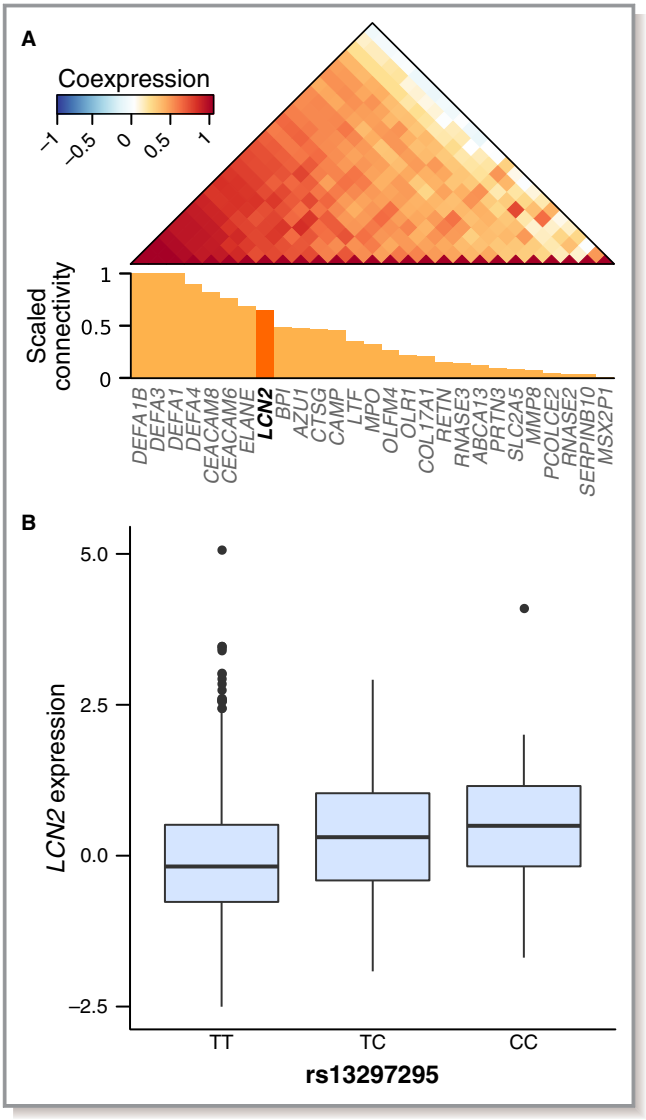

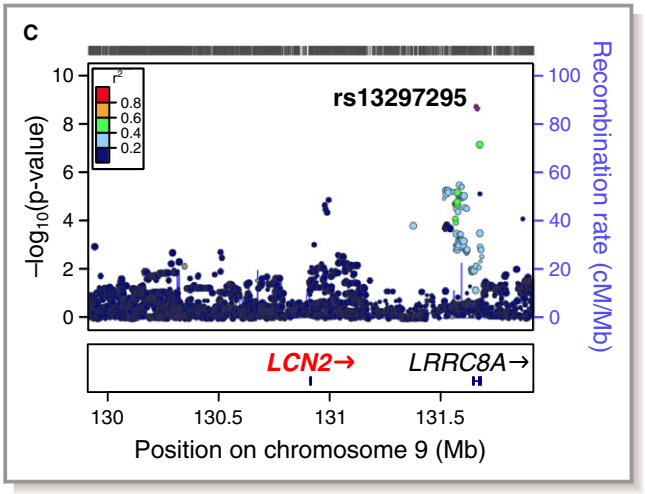

Figure 7. Continued

Figure 7. Neutrophil module: An inflammatory biomarker associated coexpression network is under genetic control of a *cis*-eQTL of lipocalin-2 (*LCN2*). A, coexpression heatmap (Spearman's correlation) and scaled network connectivity (Methods) of genes composing the neutrophil module in the YFS (n=1650). B, Box plots of age- and sex-adjusted *LCN2* expression in individuals with differing dosages of the rs13297295 minor allele ("C"). C, Locus zoom plot of the 1-MB region around *LCN2* showing association on the *y*-axis ($-\log_{10}$ *P* value) between each single-nucleotide polymorphism (points) and *LCN2* expression, recombination rate in the EUR population in that region (blue line underneath the points), and r^2 between each SNP and rs13297295 (point color).

numbers would contribute to cardiac hypertrophy. However, in very early life, when cardiomyocyte replication establishes the endowment of cardiac contractile cells, the actions of *Lcn2* to reduce cell numbers could have long-lasting effects.[46] Fewer cells means greater individual workload resulting in hypertrophy. We have shown previously that the HHR has a reduced complement of cardiomyocytes in early postnatal life, an age at which we discovered cardiac *Lcn2* to be highly expressed. Although we have no measurements of cardiomyocyte numbers in the early postnatal period following intrauterine growth restriction, other studies have shown that birth weight is associated with reduced numbers of cardiomyocytes,[47] and very early protein restriction has been associated with increased cardiomyocyte apoptosis.[48] Therefore, increased *Lcn2* very early in life (whether genetic or environmental in origin) could predispose to hypertrophy through effects on cell number. The propensity for hypertrophy would be magnified by any persistent increase in *Lcn2* levels into adulthood, as we saw in the HHR and in adult animals that had experienced intrauterine growth retardation.

In our human analyses, we found that LCN2 expression correlated significantly with cardiac size in healthy subjects in the YFS. Cardiac size also correlated with BMI in these subjects. Increased BMI is known to augment LCN2, probably as part of the induction of a chronic mild inflammatory state.[49] Given the direct effects of LCN2 on cardiomyocyte hypertrophy, it is not unreasonable to suggest that at least part of the influence of BMI on heart size might be mediated through increases in LCN2. Diabetes mellitus is also characterized as a state of chronic inflammation and cardiac hypertrophy is a common finding patients with type 2 diabetes mellitus.[50] We found that diabetic patients with cardiac hypertrophy had significantly higher plasma concentrations of LCN2, even after adjustment of BMI, renal function, and blood pressure. In the absence of other measures of inflammatory markers, we cannot be certain of the explanation of the elevated LCN2 in those diabetics with cardiac hypertrophy.

The factors that might increase LCN2 deserve consideration. LCN2 exhibits complex and tissue-specific regulation and pathophysiology relevant to a broad portfolio of biological functions and disease involvements, including bacterial

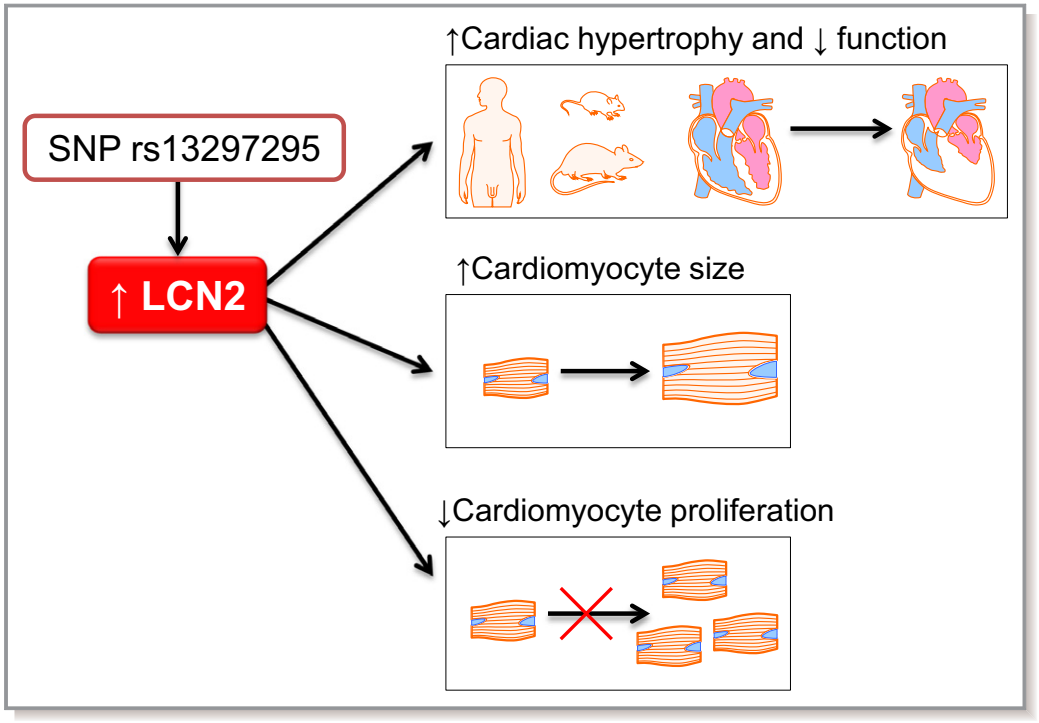

Figure 8. Diagram showing summary of findings. LCN2 indicates lipocalin-2; SNP, single-nucleotide polymorphism.

infection, inflammation, cancer, renal damage, obesity, and, more recently, CVD.[51]

In the YFS, the associations between LCN2 and the biomarkers, CRP and GlycA, suggest that underlying activation of inflammatory pathways might be responsible. LCN2 is released from neutrophils in response to inflammatory cytokines, including tumor necrosis factor-α, interleukin-1β and interleukin-6.[51] We analyzed the transcriptional subnetworks associated with the biomarkers of low-grade inflammation in otherwise healthy individuals of the YFS. LCN2 expression appeared central to a coexpression module representing proteins secreted or expressed by neutrophils as part of the innate immune response.[32] The expression of this neutrophil module was significantly associated with levels of both CRP and GlycA. Expression QTL analyses identified a common human genetic variant that increased *LCN2* levels (rs13297295 "C" allele) and was also positively associated with module expression. Despite limited power to detect hypertrophic phenotype associations, further studies of this *LCN2* eQTL in human cardiomyocytes is warranted.

In relation to increased *Lcn2* expression in the HHR, evidence of underlying activation of inflammatory pathways is less clear. We could find no significant differential cardiac expression in neonatal HHR of the cytokines, tumor necrosis factor-α, interleukin-1β, or interleukin-6, or the acute-phase reactants that comprise the majority of GlycA (data not shown). Nor was there any significant association of Lcn2 with MMP9 expression. Given the polygenic nature of the HHR, other genetic factors are presumed to drive the higher *Lcn2* expression. In a simple candidate gene approach, we identified 3 differences in DNA sequence in and around the *Lcn2* gene between HHR and NHR, 1 of which (rs196968512) created a binding site for the transcriptional enhancer, RAR-related orphan receptor A. The significance of this SNP and other polymorphisms requires further investigation in cross-breeding linkage analyses.

The downstream effects of Lcn2 on cardiac expression pathways were reasonably consistent with changes in the pathways typically associated with hypertrophy observed in the HHR, the *Lcn2* knockout mice, and in cultured cardiomyocytes. Of particular interest, in vitro *Lcn2* overexpression downregulated the genes for dynamin 1 and thrombospondin 2 in cardiomyocytes. Mice with a mutation in the gene for dynamin 1 develop dilated cardiomyopathy through mitochondria defect and thus energy deficiency in the heart.[40] thrombospondin 2-knockout mice also display dilated cardiomyopathy with progressive cardiomyocyte stress and death.[41]

Our findings add to the evidence supporting a role for LCN2 in CVD, likely through inflammatory processes. Previous studies have shown LCN2 to be associated with atherosclerosis and plaque instability, endothelial dysfunction, oxidative stress,[52] interstitial fibrosis,[53] myocarditis, cardiac remodeling, and heart failure.[54,55] Baseline circulating LCN2 levels

have been independently associated with subsequent development of CVD in 1 population study[56] and in a 4-year follow-up after cerebrovascular ischemia study.[57]

Perspectives

The actions of LCN2 that we have observed on cardiomyocyte division and growth have implications for the development of cardiac hypertrophy and failure. The timing of the actions of LCN2 is also important. In the perinatal period, LCN2 could reduce the endowment of cardiomyocytes. In adulthood, LCN2 would tend to augment cardiomyocyte hypertrophy in response to any form of myocardial injury. The stimuli to LCN2 expression are both genetic—as in the HHR polygenic model in rats and possibly in the case of rs13297295 in man—and also environmental, as in the case of early-life deprivation or other inflammatory activators, such as obesity and type 2 diabetes mellitus. Unfortunately, there are no human data regarding LCN2 in the neonatal period, and it is yet to be determined whether adult human cardiac hypertrophy might have its origin in reduced numbers of cardiomyocytes, but this emerges as a fascinating and important possibility.

Acknowledgments

We thank the Ramaciotti Centre for Gene Function Analysis for the help with arrays and the Australian Genome Research Facility for the help with Sanger and next-generation sequencing. The authors thank Irina Lisinen for the expert technical assistance in the statistical analyses.

Sources of Funding

This work was supported by grants from the National Health & Medical Research Council of Australia (project grant APP1034371, APP509252), the National Heart Foundation (project grant G10M5155, GM6368), and the Federation University Australia "Self-sustaining Regions Research and Innovation Initiative," an Australian Government Collaborative Research Network (CRN). Marques is supported by NHMRC (APP1052659) and National Heart Foundation (PF12M6785) co-shared Early Career Fellowships, and a National Heart Foundation Future Leader and Baker Fellowships. Prestes is supported by a Robert HT Smith Fellowship from the Federation University Australia. Patel is supported by a Melbourne University Career Development Fellowship. Inouye was supported by a Career Development Fellowship from the National Health & Medical Research Council of Australia and National Heart Foundation (APP1061435). Byars and Inouye were supported by an NHMRC Project Grant (APP1062227). Wlodek was supported by a National Health & Medical Research Council of Australia Project Grant (APP400003). Salomaa was supported by the Finnish Foundation for Cardiovascular Research. Kettunen was supported by the Academy of Finland (grant 283045). Ala-Korpela receives funds from the University of Bristol and UK Medical Research Council (MC_UU_12013/1). Würtz was supported by the Novo Nordisk Foundation. The Young Finns Study was financially supported by the Academy of Finland: grants 286284, 134309 (Eye), 126925, 121584, 124282, 129378 (Salve), 117787 (Gendi), and 41071 (Skidi); the Social Insurance Institution of Finland; Kuopio, Tampere, and Turku University Hospital Medical Funds (grant X51001); Juho Vainio Foundation; Paavo Nurmi Foundation; Finnish Foundation of Cardiovascular Research; Finnish Cultural Foundation; Tampere Tuberculosis Foundation; Emil Aaltonen Foundation; Yrjö Jahnsson Foundation; and Signe and Ane Gyllenberg Foundation. The quantitative serum NMR metabolomics platform and its development was supported by the Academy of Finland, TEKES—the Finnish Funding Agency for Technology and Innovation, Sigrid Juselius Foundation, Novo Nordisk Foundation, Finnish Diabetes Research Foundation, Paavo Nurmi Foundation, and strategic and infrastructural research funding from the University of Oulu, Finland, British Heart Foundation, Wellcome Trust, and Medical Research Council, UK.

Disclosures

Würtz, Kangas, Soininen, and Ala-Korpela are shareholders of Brainstake Ltd. (www.brainshake.fi), a company offering NMR-based metabolic profiling. Würtz, Kangas, Soininen, and Kettunen report employment for Brainstake Ltd.

References

1. Levy D, Garrison RJ, Savage DD, Kannel WB, Castelli WP. Prognostic implications of echocardiographically determined left ventricular mass in the Framingham Heart Study. *N Engl J Med*. 1990;322:1561–1566.
2. Frieler RA, Mortensen RM. Immune cell and other noncardiomyocyte regulation of cardiac hypertrophy and remodeling. *Circulation*. 2015;131:1019–1030.
3. Palmieri V, Tracy RP, Roman MJ, Liu JE, Best LG, Bella JN, Robbins DC, Howard BV, Devereux RB; Strong Heart S. Relation of left ventricular hypertrophy to inflammation and albuminuria in adults with type 2 diabetes: the Strong Heart Study. *Diabetes Care*. 2003;26:2764–2769.
4. Salles GF, Fiszman R, Cardoso CR, Muxfeldt ES. Relation of left ventricular hypertrophy with systemic inflammation and endothelial damage in resistant hypertension. *Hypertension*. 2007;50:723–728.
5. Danesh J, Collins R, Appleby P, Peto R. Association of fibrinogen, C-reactive protein, albumin, or leukocyte count with coronary heart disease: meta-analyses of prospective studies. *JAMA*. 1998;279:1477–1482.
6. Halade GV, Jin YF, Lindsey ML. Matrix metalloproteinase (MMP)-9: a proximal biomarker for cardiac remodeling and a distal biomarker for inflammation. *Pharmacol Ther*. 2013;139:32–40.
7. Blankenberg S, Rupprecht HJ, Poirier O, Bickel C, Smieja M, Hafner G, Meyer J, Cambien F, Tiret L; AtheroGene I. Plasma concentrations and genetic variation of matrix metalloproteinase 9 and prognosis of patients with cardiovascular disease. *Circulation*. 2003;107:1579–1585.
8. Folkesson M, Kazi M, Zhu C, Silveira A, Hemdahl AL, Hamsten A, Hedin U, Swedenborg J, Eriksson P. Presence of NGAL/MMP-9 complexes in human abdominal aortic aneurysms. *Thromb Haemost*. 2007;98:427–433.

9. Bu DX, Hemdahl AL, Gabrielsen A, Fuxe J, Zhu C, Eriksson P, Yan ZQ. Induction of neutrophil gelatinase-associated lipocalin in vascular injury via activation of nuclear factor-kappaB. *Am J Pathol*. 2006;169:2245–2253.
10. Bolignano D, Coppolino G, Lacquaniti A, Buemi M. From kidney to cardiovascular diseases: NGAL as a biomarker beyond the confines of nephrology. *Eur J Clin Invest*. 2010;40:273–276.
11. Leoncini G, Mussap M, Viazzi F, Fravega M, Degrandi R, Bezante GP, Deferrari G, Pontremoli R. Combined use of urinary neutrophil gelatinase-associated lipocalin (uNGAL) and albumin as markers of early cardiac damage in primary hypertension. *Clin Chim Acta*. 2011;412:1951–1956.
12. Hemdahl AL, Gabrielsen A, Zhu C, Eriksson P, Hedin U, Kastrup J, Thoren P, Hansson GK. Expression of neutrophil gelatinase-associated lipocalin in atherosclerosis and myocardial infarction. *Arterioscler Thromb Vasc Biol*. 2006;26:136–142.
13. Maisel AS, Mueller C, Fitzgerald R, Brikhan R, Hiestand BC, Iqbal N, Clopton P, van Veldhuisen DJ. Prognostic utility of plasma neutrophil gelatinase-associated lipocalin in patients with acute heart failure: the NGAL EvaLuation Along with B-type NaTriuretic Peptide in acutely decompensated heart failure (GALLANT) trial. *Eur J Heart Fail*. 2011;13:846–851.
14. Minana G, Rumiz E, Palau P, Valero E, Bodi V, Nunez E, Sanchis J, Nunez J. Plasma neutrophil gelatinase-associated lipocalin and long-term mortality in patients with acute heart failure and normal renal function. *Int J Cardiol*. 2016;214:51–53.
15. Harrap SB, Danes VR, Ellis JA, Griffiths CD, Jones EF, Delbridge LM. The hypertrophic heart rat: a new normotensive model of genetic cardiac and cardiomyocyte hypertrophy. *Physiol Genomics*. 2002;9:43–48.
16. Porrello ER, Bell JR, Schertzer JD, Curl CL, McMullen JR, Mellor KM, Ritchie RH, Lynch GS, Harrap SB, Thomas WG, Delbridge LM. Heritable pathologic cardiac hypertrophy in adulthood is preceded by neonatal cardiac growth restriction. *Am J Physiol Regul Integr Comp Physiol*. 2009;296:R672–R680.
17. Markus MA, Marques FZ, Morris BJ. Resveratrol, by modulating RNA processing factor levels, can influence the alternative splicing of pre-mRNAs. *PLoS One*. 2011;6:e28926.
18. Wlodek ME, Mibus A, Tan A, Siebel AL, Owens JA, Moritz KM. Normal lactational environment restores nephron endowment and prevents hypertension after placental restriction in the rat. *J Am Soc Nephrol*. 2007;18:1688–1696.
19. Wlodek ME, Westcott K, Siebel AL, Owens JA, Moritz KM. Growth restriction before or after birth reduces nephron number and increases blood pressure in male rats. *Kidney Int*. 2008;74:187–195.
20. Porrello ER, Johnson BA, Aurora AB, Simpson E, Nam YJ, Matkovich SJ, Dorn GW II, van Rooij E, Olson EN. MiR-15 family regulates postnatal mitotic arrest of cardiomyocytes. *Circ Res*. 2011;109:670–679.
21. Robinson MD, McCarthy DJ, Smyth GK. edgeR: a Bioconductor package for differential expression analysis of digital gene expression data. *Bioinformatics*. 2010;26:139–140.
22. Srivastava PM, Calafiore P, Macisaac RJ, Patel SK, Thomas MC, Jerums G, Burrell LM. Prevalence and predictors of cardiac hypertrophy and dysfunction in patients with Type 2 diabetes. *Clin Sci (Lond)*. 2008;114:313–320.
23. Raitakari OT, Juonala M, Ronnemaa T, Keltikangas-Jarvinen L, Rasanen L, Pietikainen M, Hutri-Kahonen N, Taittonen L, Jokinen E, Marniemi J, Jula A, Telama R, Kahonen M, Lehtimaki T, Akerblom HK, Viikari JS. Cohort profile: the cardiovascular risk in Young Finns Study. *Int J Epidemiol*. 2008;37:1220–1226.
24. Raitoharju E, Seppala I, Oksala N, Lyytikainen LP, Raitakari O, Viikari J, Ala-Korpela M, Soininen P, Kangas AJ, Waldenberger M, Klopp N, Illig T, Leiviska J, Loo BM, Hutri-Kahonen N, Kahonen M, Laaksonen R, Lehtimaki T. Blood microRNA profile associates with the levels of serum lipids and metabolites associated with glucose metabolism and insulin resistance and pinpoints pathways underlying metabolic syndrome: the cardiovascular risk in Young Finns Study. *Mol Cell Endocrinol*. 2014;391:41–49.
25. Smith EN, Chen W, Kahonen M, Kettunen J, Lehtimaki T, Peltonen L, Raitakari OT, Salem RM, Schork NJ, Shaw M, Srinivasan SR, Topol EJ, Viikari JS, Berenson GS, Murray SS. Longitudinal genome-wide association of cardiovascular disease risk factors in the Bogalusa heart study. *PLoS Genet*. 2010;6:e1001094.
26. Wurtz P, Wang Q, Kangas AJ, Richmond RC, Skarp J, Tiainen M, Tynkkynen T, Soininen P, Havulinna AS, Kaakinen M, Viikari JS, Savolainen MJ, Kahonen M, Lehtimaki T, Mannisto S, Blankenberg S, Zeller T, Laitinen J, Pouta A, Mantyselka P, Vanhala M, Elliott P, Pietilainen KH, Ripatti S, Salomaa V, Raitakari OT, Jarvelin MR, Smith GD, Ala-Korpela M. Metabolic signatures of adiposity in young adults: Mendelian randomization analysis and effects of weight change. *PLoS Med*. 2014;11:e1001765.
27. Ruohonen S, Koskenvuo JW, Wendelin-Saarenhovi M, Savontaus M, Kahonen M, Laitinen T, Lehtimaki T, Jokinen E, Viikari J, Juonala M, Taittonen L, Tossavainen P, Kallio M, Bax JJ, Raitakari O. Reference values for echocardiography in middle-aged population: the cardiovascular risk in Young Finns Study. *Echocardiography*. 2016;33:193–206.
28. Lang RM, Bierig M, Devereux RB, Flachskampf FA, Foster E, Pellikka PA, Picard MH, Roman MJ, Seward J, Shanewise JS, Solomon SD, Spencer KT, Sutton MS, Stewart WJ; Chamber Quantification Writing G, American Society of Echocardiography's G, Standards C and European Association of E. Recommendations for chamber quantification: a report from the American Society of Echocardiography's Guidelines and Standards Committee and the Chamber Quantification Writing Group, developed in conjunction with the European Association of Echocardiography, a branch of the European Society of Cardiology. *J Am Soc Echocardiogr*. 2005;18:1440–1463.
29. Maragiannis D, Nagueh SF. Echocardiographic evaluation of left ventricular diastolic function: an update. *Curr Cardiol Rep*. 2015;17:3.
30. Wai B, Patel SK, Ord M, MacIsaac RJ, Jerums G, Srivastava PM, Burrell LM. Prevalence, predictors and evolution of echocardiographically defined cardiac abnormalities in adults with type 1 diabetes: an observational cohort study. *J Diabetes Complications*. 2014;28:22–28.
31. Otvos JD, Shalaurova I, Wolak-Dinsmore J, Connelly MA, Mackey RH, Stein JH, Tracy RP. GlycA: a composite nuclear magnetic resonance biomarker of systemic inflammation. *Clin Chem*. 2015;61:714–723.
32. Ritchie SC, Wurtz P, Nath AP, Abraham G, Havulinna AS, Fearnley LG, Sarin AP, Kangas AJ, Soininen P, Aalto K, Seppala I, Raitoharju E, Salmi M, Maksimow M, Mannisto S, Kahonen M, Juonala M, Ripatti S, Lehtimaki T, Jalkanen S, Perola M, Raitakari O, Salomaa V, Ala-Korpela M, Kettunen J, Inouye M. The biomarker GlycA is associated with chronic inflammation and predicts long-term risk of severe infection. *Cell Syst*. 2015;1:293–301.
33. Bell JD, Brown JC, Nicholson JK, Sadler PJ. Assignment of resonances for 'acute-phase' glycoproteins in high resolution proton NMR spectra of human blood plasma. *FEBS Lett*. 1987;215:311–315.
34. Shi W, Oshlack A, Smyth GK. Optimizing the noise versus bias trade-off for Illumina whole genome expression BeadChips. *Nucleic Acids Res*. 2010;38:e204.
35. Ritchie SC, Watts S, Fearnley LG, Holt KE, Abraham G, Inouye M. A scalable permutation approach reveals replication and preservation of network modules. *Cell Syst*. 2016;3:71–82.
36. Thomas-Chollier M, Hufton A, Heinig M, O'Keeffe S, Masri NE, Roider HG, Manke T, Vingron M. Transcription factor binding predictions using TRAP for the analysis of ChIP-seq data and regulatory SNPs. *Nat Protoc*. 2011;6:1860–1869.
37. Manke T, Heinig M, Vingron M. Quantifying the effect of sequence variation on regulatory interactions. *Hum Mutat*. 2010;31:477–483.
38. Giguere V, Tini M, Flock G, Ong E, Evans RM, Otulakowski G. Isoform-specific amino-terminal domains dictate DNA-binding properties of ROR alpha, a novel family of orphan hormone nuclear receptors. *Genes Dev*. 1994;8:538–553.
39. Flo TH, Smith KD, Sato S, Rodriguez DJ, Holmes MA, Strong RK, Akira S, Aderem A. Lipocalin 2 mediates an innate immune response to bacterial infection by sequestrating iron. *Nature*. 2004;432:917–921.
40. Ashrafian H, Docherty L, Leo V, Towlson C, Neilan M, Steeples V, Lygate CA, Hough T, Townsend S, Williams D, Wells S, Norris D, Glyn-Jones S, Land J, Barbaric I, Lalanne Z, Denny P, Szumska D, Bhattacharya S, Griffin JL, Hargreaves I, Fernandez-Fuentes N, Cheeseman M, Watkins H, Dear TN. A mutation in the mitochondrial fission gene Dnm1 l leads to cardiomyopathy. *PLoS Genet*. 2010;6:e1001000.
41. Swinnen M, Vanhoutte D, Van Almen GC, Hamdani N, Schellings MW, D'Hooge J, Van der Velden J, Weaver MS, Sage EH, Bornstein P, Verheyen FK, VandenDriessche T, Chuah MK, Westermann D, Paulus WJ, Van de Werf F, Schroen B, Carmeliet P, Pinto YM, Heymans S. Absence of thrombospondin-2 causes age-related dilated cardiomyopathy. *Circulation*. 2009;120:1585–1597.
42. Yan QW, Yang Q, Mody N, Graham TE, Hsu CH, Xu Z, Houstis NE, Kahn BB, Rosen ED. The adipokine lipocalin 2 is regulated by obesity and promotes insulin resistance. *Diabetes*. 2007;56:2533–2540.
43. Taube A, Schlich R, Sell H, Eckardt K, Eckel J. Inflammation and metabolic dysfunction: links to cardiovascular diseases. *Am J Physiol Heart Circ Physiol*. 2012;302:H2148–H2165.
44. Poornima IG, Parikh P, Shannon RP. Diabetic cardiomyopathy: the search for a unifying hypothesis. *Circ Res*. 2006;98:596–605.
45. Galderisi M, Benjamin EJ, Evans JC, D'Agostino RB, Fuller DL, Lehman B, Levy D. Impact of heart rate and PR interval on Doppler indexes of left ventricular diastolic filling in an elderly cohort (the Framingham Heart Study). *Am J Cardiol*. 1993;72:1183–1187.
46. Ahuja P, Sdek P, MacLellan WR. Cardiac myocyte cell cycle control in development, disease, and regeneration. *Physiol Rev*. 2007;87:521–544.

47. Stacy V, De Matteo R, Brew N, Sozo F, Probyn ME, Harding R, Black MJ. The influence of naturally occurring differences in birthweight on ventricular cardiomyocyte number in sheep. *Anat Rec (Hoboken)*. 2009; 292:29–37.
48. Cheema KK, Dent MR, Saini HK, Aroutiounova N, Tappia PS. Prenatal exposure to maternal undernutrition induces adult cardiac dysfunction. *Br J Nutr*. 2005;93:471–477.
49. Wang Y, Lam KS, Kraegen EW, Sweeney G, Zhang J, Tso AW, Chow WS, Wat NM, Xu JY, Hoo RL, Xu A. Lipocalin-2 is an inflammatory marker closely associated with obesity, insulin resistance, and hyperglycemia in humans. *Clin Chem*. 2007;53:34–41.
50. Donath MY, Shoelson SE. Type 2 diabetes as an inflammatory disease. *Nat Rev Immunol*. 2011;11:98–107.
51. Chakraborty S, Kaur S, Guha S, Batra SK. The multifaceted roles of neutrophil gelatinase associated lipocalin (NGAL) in inflammation and cancer. *Biochim Biophys Acta*. 2012;1826:129–169.
52. Chan YK, Sung HK, Sweeney G. Iron metabolism and regulation by neutrophil gelatinase-associated lipocalin in cardiomyopathy. *Clin Sci (Lond)*. 2015;129:851–862.
53. Tarjus A, Martinez-Martinez E, Amador C, Latouche C, El Moghrabi S, Berger T, Mak TW, Fay R, Farman N, Rossignol P, Zannad F, Lopez-Andres N, Jaisser F. Neutrophil gelatinase-associated lipocalin, a novel mineralocorticoid biotarget, mediates vascular profibrotic effects of mineralocorticoids. *Hypertension*. 2015;66:158–166.
54. Daniels LB, Barrett-Connor E, Clopton P, Laughlin GA, Ix JH, Maisel AS. Plasma neutrophil gelatinase-associated lipocalin is independently associated with cardiovascular disease and mortality in community-dwelling older adults: the Rancho Bernardo Study. *J Am Coll Cardiol*. 2012;59:1101–1109.
55. Alvelos M, Lourenco P, Dias C, Amorim M, Rema J, Leite AB, Guimaraes JT, Almeida P, Bettencourt P. Prognostic value of neutrophil gelatinase-associated lipocalin in acute heart failure. *Int J Cardiol*. 2013;165:51–55.
56. Wu G, Li H, Fang Q, Jiang S, Zhang L, Zhang J, Hou X, Lu J, Bao Y, Xu A, Jia W. Elevated circulating lipocalin-2 levels independently predict incident cardiovascular events in men in a population-based cohort. *Arterioscler Thromb Vasc Biol*. 2014;34:2457–2464.
57. Falke P, Elneihoum AM, Ohlsson K. Leukocyte activation: relation to cardiovascular mortality after cerebrovascular ischemia. *Cerebrovasc Dis*. 2000;10:97–101.

Supplemental Material

Data S1.

Supplemental Methods

Animal Samples

We then studied the hypertrophic heart rat (HHR) as a normotensive inbred polygenetic model of adult cardiac hypertrophy and failure that begins life with a smaller heart and fewer cells[1, 2]. Neonatal male (day 2, n=11 HHR, n=10 NHR), adolescent (4-week old, n=4 HHR and n=4 NHR for cardiomyocyte isolation), young adult (13 weeks-old, n=7 HHR, n=7 NHR) and old adult (50 weeks-old, n=11 HHR, n=10 NHR) age-matched animals were euthanized by decapitation (neonatal) or with an overdose of pentobarbitone (Lethobarb) (adult animals). The heart was immediately removed, and the ventricles were dissected from the atriums. Cardiac weight index (CWI, mg/g) was calculated from the total heart weight (mg) relative to total body weight (g) of the animal. HHR samples presented hypertrophy since 4 weeks of age (data not shown). Plasma was also collected. An environmental model of left ventricular hypertrophy developed using Wistar Kyoto (WKY) rats by intra-uterine growth restriction induced by uteroplacental insufficiency on day 18 of pregnancy (term=22 days) was also investigated [3, 4]. Six month old male operated animals (n=3) were compared to WKY sham rats (n=7). For all samples, the tissues used were first preserved in liquid nitrogen and later transferred to a –80ºC freezer, and RNA was extracted using miRNeasy kit (Qiagen). Based on the means and standard deviation reported in the manuscript, the number of samples used resulted in power >95% for both t-test and analysis of variance (ANOVA), as calculated using the software G*Power version 3.0.10 (http://www.gpower.hhu.de). The study was approved by the Animal Ethics Committee of the University of Melbourne and Deakin University, and ratified at Federation University Australia.

Microarray Experiments and Analyses

Total RNA was extracted from left ventricle of neonatal HHR (4 male, 4 female) and NHR (4 male, 4 female) using the miRNeasy Mini kit (Qiagen). Affymetrix GeneChip® Rat Gene 1.0 ST Arrays were used for transcriptome-wide gene expression analysis. Each animal was considered an individual sample and no pooling was performed. Briefly, mRNA was converted to ssDNA, labelled and hybridized to GeneChip® Rat Gene 1.0 ST Arrays, which analyse 27,342 gene transcripts using 722,254 probe sets (on average 26 probes per gene), according to the manufacturer's instructions, and with the assistance of the Ramaciotti Centre for Gene Function Analysis (University of New South Wales, Sydney, Australia). The data set obtained has been deposited in the NCBI Gene Expression Omnibus (GEO) database according to MIAMI guidelines with series accession number GSE38607 (http://www.ncbi.nlm.nih.gov/geo/query/acc.cgi?token=bjsxbiiaowmwozy&acc=GSE38607).

Results from arrays were normalized using robust-multi-array analysis (RMA). Differentially expressed genes were identified using a two-sample t-test in the Partek® Genomics Suite™ (version 6.6). Such genes were selected based on their Bonferroni-adjusted *P*-value <0.05 and fold difference higher than 2. Hierarchical clustering using Euclidean distance with all genes with Bonferroni *P*-value<0.05 was performed with Partek® Genomics Suite™. Gene Ontology (GO), used to further interpret the differentially expressed gene data set and to identify over-represented functional groups of genes, and Gene Set Enrichment Analysis (GSEA), used to highlight pathways over- or under-represented as a set, were also performed in Partek. Molecular networks related to differentially expressed genes were built via the Ingenuity Pathway Analysis (IPA, Ingenuity® Systems, www.ingenuity.com) application using the "Core Analysis" function. Briefly, a data set

containing differentially expressed genes and respective fold differences were first uploaded into the application. The genes were then correlated based on previous association between genes or proteins and known functional roles of genes. The biological relationship between two genes, represented as nodes, is shown as a line. Nodes with different shapes indicate different functional class.

Isolation of cardiomyocytes and other cells

Cardiomyocytes were isolated from whole NHR and HHR hearts as we previously described [2]. After 10 min incubation, cardiomyocytes were deposited in the bottom of tubes. The supernatant was considered to contain other cells than cardiomyocytes. Cardiomyocytes or other cells were pelleted by centrifugation at 4,000 RCF for 5 min in a refrigerated bench top centrifuge. Total RNA was extracted from both cardiomyocytes and other cells for each sample using the miRNeasy kit (Qiagen) as described above. cDNA and qPCR were performed as described above.

Real-time Quantitative PCR (qPCR)

First-strand complementary synthesis reaction was performed using the High Capacity cDNA Reverse Transcription Kit (Life Technologies). Primers were designed to flank an exon-exon junction using Primer3 [5] and NCBI tool Primer Blast. Primers and conditions used for all qPCR are shown in Online Table 1. Amplification reactions used the SensiFast™ SYBR Low-ROX Kit qPCR reagent system (Bioline) in a Viia7 qPCR instrument (Life Technologies). Samples were run in duplicates. The specificity of the qPCR was ensured by melting curve analysis and electrophoresis in agarose gels (data not shown). The glyceraldehyde 3-phosphate dehydrogenase (*Gapdh*) was used as reference transcript. Significance was assessed by $2^{-\Delta\Delta C_T}$ method [6].

Plasma measurement of LCN2

In animal samples, after euthanasia, blood was immediately collected in EDTA tubes and centrifuged. Plasma was stored separately. Lcn2 plasma and left ventricle levels were measured by enzyme-linked immunosorbent assay (ELISA) in duplicates in neonatal and adult HHR and NHR using the Lipocalin-2 Rat ELISA Kit (Abcam) according to the supplier. Human plasma collected in heparin tubes was used to measure LCN2 levels using the Quantikine ELISA Human Lipocalin-2 Immunoassay (R&D Systems) according to the supplier. Inter- and intra-assay coefficients of variability were calculated and only less than 15% variability was accepted (hence 7 human samples were excluded from further analyses). The overall intra-assay coefficient was 4.3% and the inter-coefficient was 4.5%.

Immunohistochemistry

Immunohistochemistry was performed using an anti-LCN2 Rabbit Polyclonal antibody (1:200 dilution, OriGene Technologies, TA322583), followed by the EnVision+System-HRP (Dako). In immunohistochemistry images, the positive staining (Lcn2) was the standard brown while the counterstain was haematoxylin (stains blue). Images were obtained in an EVOS® XL Cell Imaging System (Life Technologies) microscope using a 400x magnification.

Protein measurement of Lcn2 by Western Blots

Protein was extracted from left ventricle of 13 week old HHR and NHR by the use of RIPA buffer (Sigma-Aldrich) and 1% Halt Protease & Phosphatase Inhibitor Cocktail (Thermo Scientific). Fifty micrograms of extracted rat proteins were resolved by 4–15% Mini-PROTEAN® TGX™ Precast Gel (BioRad). Proteins were electroblotted on to a Nitrocellulose Membrane (Thermo Scientific). Membranes were blocked for two hours in 5%

skim milk, then incubated overnight at 4ºC with Anti-LCN2 Rabbit Polyclonal antibody (1:2500 dilution, OriGene Technologies, TA322583) or β-actin (1:5000 dilution, Cell Signalling, 3700) in blocking solution, followed by several washing steps in PBS-Tween 20, 1 h at RT with secondary antibody (Lcn2: Anti-rabbit HRP-linked Antibody, 1:5000 dilution, Cell Signalling, 7074S; and β-actin: Anti-mouse HRP-linked Antibody, 1:5000 dilution, Cell Signalling, 7076S) in blocking solution, and several washing steps in PBS-Tween 20, before detection by enhanced chemiluminescence SuperSignal West Pico Substrate (Thermo Scientific) according to the manufacturer's instructions. Images were captured with a UVITEC Alliance digital imaging system (Thermo Scientific). Bands were quantified using Image J software, and Lcn2 protein levels were calculated as a ratio relative to β-actin. Both 25 kDa monomer Lcn2 and Lcn2 complexed with matrix metallopeptidase 9 (Mmp9) were measured.

DNA sequencing

Sanger sequencing was used to sequence 10,000 base pairs (bp) before and 2,000 bp after the Lcn2 gene (primers and conditions in Online Table 1). Briefly we extracted DNA using PureLink® Genomic Extraction kit (Life Technologies), and then amplified it with IMMOLASE DNA Polymerase (Bioline) in a themocycler (BioRad). PCR fragments were purified using the Wizard® SV Gel and PCR Clean-Up System (Promega) and send out for sequencing at AGRF. We sequenced the DNA of both HHR and NHR and align them to the sequence of both SHR and Fisher 344 (the two strains which originated the HHR and NHR), and the reference genome from the Rat Genome Database (version 5).

Lcn2-knockout

Whole body and heart size of adult (12-13 week-old) whole-body *Lcn2* knockout (*Lcn2*-KO, n=6) and age-matched wild-type mice C57BL/6 (n=4) were measured upon death, and CWI was calculated as described above. Both *Lcn2*-KO and wild-type mice were sourced from Prof Alan Aderem (University of Washington) [7].

Vector containing Lcn2

The pExpress vector containing the cDNA for the rat Lcn2 (Thermo Scientific, catalogue number ID MRN1768-98079404) was transformed into JM109 competent cells (Promega). Constructs were cultivated in plates of Luria-Bertani (LB) medium containing agar and ampicillin (50 μg/ml). Individual colonies were selected and the presence of the vector was confirmed by restriction enzyme and Sanger sequencing. The colonies containing the vector were cultured in LB medium overnight, and plasmids were extracted using a PureLink™ HiPure Plasmid Filter Kit (Life Technologies). To create an empty pExpress vector to be used as a control, Lcn2 sequence was cut out of the plasmid using the restriction enzymes *Not1* and *SmaI* (Promega). DNA Polymerase I Large (Klenow) Fragment (Promega) was used to generate blunted ends. The product was run in a 1% agarose gel, and the band of the correct size was purified from the gel using the Wizard SV Gel and PCR Clean-Up system (Promega). 163 ng of this purification was ligated using T4 DNA Ligase (Life Technologies), and this was transformed into competent cells as described above. The sequence of both plasmids has been confirmed by Sanger DNA sequencing using T7 and sp6 universal primers as a service at the Australian Genome Research Facility (AGRF) as a service.

H9c2 Cell Transfections

The rat embryonic ventricular myocardial cells (H9c2: ATCC® CRL1446™) were grown in Dulbecco's modified Eagle's medium (DMEM), containing 10% fetal bovine serum (FBS) (all from Life Technologies) at 37ºC with 5% CO_2. Cell culture medium was replaced every 48–72 hours. This cell line was specifically chosen because it has similar hypertrophic

properties as rat primary neonatal cardiomyocytes.[8] The cells were purchased from ATCC, and short tandem repeats (STR) profiling was not available for this rat cell line. Moreover, cells were regularly tested for mycoplasma contamination using Hoechst staining (Life Technologies) and a Nikon C2 confocal microscope, with negative results during experiments. H9c2 cells were cultured in 6- to 24-well plates and transfected with 2ng/ml of Lcn2 or empty (pExpress only) plasmid using Lipofectamine 2000™ (Life Technologies) in cells at 50% confluence. Untransfected and mock controls were also included. Preliminary experiments were used to determine the best concentration of cells, reagents and vector to have similar levels of Lcn2 as in HHR, so copying physiological levels (Fig. S6). The minimum concentration of vector and transfection reagents, according to the manufacturer's recommendations, were used. All *in vitro* experiments were independently repeated 3 times, each time in triplicates (i.e., total of 9 biological replicates). Experiments always included Lcn2 vector, empty plasmid, untransfected cells and a positive control.

RNA-sequencing and molecular pathways

Total RNA was extracted from whole snap-frozen hearts of Lcn2-KO mice and cells transfected with Lcn2 plasmid for 48h (and respective controls) using the miRNeasy Mini kit (Qiagen). The RNA from 3 samples of each group was sent to RNA-sequencing at AGRF according to the manufacturer's instructions using the Illumina HiSeq platform (v3 chemistry 100bp paired-end sequencing). Each sample was considered an individual sample and no pooling was performed.

Read quality was assessed using the FastQC software version 0.10.1 (www.bioinformatics.babraham.ac.uk/projects/fastqc/), revealing high quality sequence and base scores (mean PHRED scores: overall=35.8, 1bp start=32.4, 100bp end=31.5), and thus read trimming was not applied. Analysis of differential expression was performed in the R statistical programming environment (version 3.1.0) using Rsubread (version 1.14.2) and edgeR (version 3.6.8) Bioconductor packages [9]. Paired-end 100bp Illumina reads were aligned to mouse (UCSC mm10 assembly) and rat genomes (UCSC rn5 assembly) at the gene-level using Rsubread aligner with 82.4% and 92.1% of reads successfully mapped overall for mouse and rat samples, respectively. For individual sample and alignment characteristics (i.e. number of paired reads, % mapped, indels, etc) see Online Table 2.

Differential expression (DE) of genes was assessed with edgeR. Genes with 1-count-per-million mapped reads or less in at least one of the samples were filtered out due to unreliable data in any sample. Count data was then normalized by finding a set of scaling factors for the library sizes that adjust for compositional differences between samples and also help account for any biases due to changes in highly expressed genes [10]. Scaling factors were calculated using the trimmed mean of M values (TMM) method [9, 11]. Biological coefficient of variation (BCV) was estimated using the common dispersion method (negative binomial dispersion by conditional maximum likelihood) for both mouse (BCV=0.250) and rat (BCV=0.023) samples. Both values were above the threshold (BCV=0.01) suggested for technical replicates in the edgeR User's Guide indicating sufficient biological variability for analysis. BCV is derived from total CV, which is the sum of estimated true biological (BCV) and technical variation (i.e. measurement error) across libraries. Gene-specific dispersions were then estimated using the empirical Bayes method (tagwise negative binomial) where expression differences that are consistent between replicates are more highly weighted than those that are not, which is necessary so that DE is not driven by outliers. DE was calculated by computing genewise exact tests for differences in the means between both groups (wild-type and knockout in mouse, control and transfected in rat) of negative-binomially distributed counts in edgeR. *P*-values were adjusted for multiple testing using the Benjamini-Hochberg

correction [12] with a FDR<0.05.

To check experimental data quality with sample clustering and heatmaps, variance stabilized expression values (i.e. normalized for variation library size/sequencing depth) were generated using the R package DESeq (version 1.16.0) [13]. This data was entered for the top 100 (ranked by unadjusted *P*-value, all *P*<0.01) differentially expressed genes into principal component analysis (PCA), hierarchical cluster analysis (HCA), gene-gene heatmap and gene-sample heatmap analysis in R. PCA and HCA confirmed control and experimental group differences (data not shown) and also provided further insight into genes that are associated with the main experimental manipulations in both the rat and mouse studies.

GO enrichment analysis was performed on filtered lists (all genes with unadjusted edgeR *P*-value<0.05, including 529 and 721 rat and mouse genes, respectively) of differentially expressed genes using Database for Annotation, Visualization and Integrated Discovery (DAVID) [14, 15] to ask which Kyoto Encyclopedia of Genes and Genomes (KEGG) pathways were enriched in genes differentially expressed in both mouse and rat samples. Circular plots were produced with the R package Rcircos (version 1.1.2) [16] and show the top 100 differentially expressed genes ranked by edgeR *P*-value and enriched pathways identified in KEGG.

Number of cells and cell size

We counted the number of cells after 48 hours of transfection by haemocytometry with the use of a Countess® Automated Cell Counter (Life Technologies). Wheat germ agglutinin (WGA) and Hoechst staining were performed as previously described to measure cell size [17]. Cell size was measured in 10 different fields per slide obtained in a Nikon C2 confocal microscope using a 400x magnification. 823 cells in average were measured for each condition. Angiotensin II (Sigma-Aldrich) added to the cells for 48h at final concentration of 0.1 μM was used as a positive control.

Cell cycle arrest

To estimate cell proliferation, we counted phospho-histone H3 (pH3) stained cells after transfection with Lcn2 vector as described above. 500 nM of colcemid (Merck Biosciences), added 2 hours before fixing cells, was used as positive control. Briefly, cells on 12mm poly-D-lysine/laminin coated coverslips were stained with pH3 and DAPI for fluorescence imaging as described somewhere else [18]. We used the primary pH3 anti-rabbit antibody (Millipore, Cat# 06-570, 1:100 dilution) and secondary goat anti-rabbit AlexaFluor-488 antibody (Invitrogen, 1:500 dilution). Ten images per slide were obtained in a Nikon C2 confocal microscope using a 200x magnification (Fig. S7).

Apoptosis

Cell death and apoptosis were measured by flow cytometry using an Annexin-V: FITC Apoptosis Detection Kit I (BD Pharmingen, Cat No. 556547). Cells were detached from plate by mild trypsinization (Life Technologies) and were washed twice with cold phosphate buffer saline (PBS). Cells were then resuspended in binding buffer and stained with annexin-V-FITC and propidium iodide as per manufacturer's protocol. The stained cells were analysed using FACS Aria II (BD Biosciences). The data analysis was performed using FCS express (version 4) research edition analytical software. 100 nM staurosporine was used as a positive control.

Human Samples

Two independent cohorts were used (Online Tables 3 and 4). One hundred and twenty one subjects were selected from a prospective cohort of type-2 diabetes (Online Table 3) [19]. Left

ventricle (LV) structure and function was studied using transthoracic echocardiography – Acuson Sequoia 512 (Acuson, Mountain View, CA, USA) with 3.5 MHz scanning frequency phased-array transducer. From the ultrasound images, LV structure, systolic and diastolic function were measured following the guidelines of American Society of Echocardiography, as previously described [20, 21]. Cardiac hypertrophy was defined as LV mass indexed to the body surface of > 95 g/m^2 in women and > 115 g/m^2 in men [19]. E/E'- ratio was calculated using the average values of lateral and septal e' velocity [21]. Other phenotypes, including blood pressure, were also available. Subjects with chronic kidney disease were excluded due to previous association with LCN2 in the literature [22]. Plasma samples were collected in heparin tubes, and stored at –80 ºC. All subjects gave informed consent and the study was approved by human ethics committee at the Austin Hospital, and ratified at Federation University Australia.

The Cardiovascular Risk in Young Finns Study (YFS) is an ongoing population-based prospective study started in 1980 to study the emergence and progression of cardiovascular disease risk factors from childhood [23]. 4,320 individuals from six age groups (3, 6, 9, 12, 15, and 18 years of age) were randomly recruited from the five major population centres of Finland (Helsinki, Kuopio, Turku, Oulu, and Tampere). A total of 3,596 individuals participated in the original study and 2,064 individuals responded to the 2011 follow-up study. Transcriptome-wide microarray profiling, genome-wide genotyping, GlycA, and echocardiography measurements were available for subsets of these 2,064 individuals [24-27]. Baseline cohort characteristics are provided in Online Table 3. Ethics were approved by the Joint Commission on Ethics of the Turku University and the Turku University Central Hospital.

Venous blood samples were collected after an overnight fast and serum samples were aliquoted and stored at –70ºC. Samples were collected after an overnight fast for the YFS cohort [23].

GlycA measurement

A proton nuclear magnetic resonance platform (Bruker AVANCE III, 500 MHz spectrometer) was used to quantify the concentrations of 106 circulating lipids, proteins, and metabolites from serum (including GlycA and total triglycerides) in the YFS cohort. Detailed experimental protocols are described in [28].

CRP measurement

High-sensitivity C-reactive protein (CRP) was quantified from YFS serum samples using an automated analyser with a latex turbidimetric immunoassay kit.

Coexpression networks and quantitative trait locus

Transcriptome wide microarray profiling was performed on whole blood for 1,650 individuals in the YFS as previously described [24]. Briefly, stabilised total RNA was obtained from whole blood for individuals in the YFS using the PAXgene Blood RNA System. An Eppendorf BioPhotometer was used to evaluate RNA concentrations and purity and the isolation process validated using an Agilent RNA 6000 Nano Chip Kit. RNA was hybridized to Illumina HT-12 (version 4) BeadChip arrays and raw probe data was exported with the Illumina BeadStudio software. Negative control probes were used to background correct the microarrays. Both positive and negative control probes were used to quantile normalised using the *limma* R package [29]. Probe intensities were reported on a $\log_2$ scale.

Coexpression was calculated for genes composing the previously described neutrophil module [30] as the Spearman correlation coefficient between the gene expression microarray

data. The average probe intensity across samples was taken for genes with multiple probes (*DEFA1B*, *OLFM4*, *COL17A1*). Edges in the interaction network were defined as the absolute value of the coexpression exponentiated to the power 4 as in [30]. The connectivity of each gene was calculated as the sum of edge weights to all other genes in the module then scaled by the connectivity of *DEFA1B*; the most connected gene. The scaled connectivity is a measure of biological importance to the network [31]. A summary profile of module expression was calculated as the first eigenvector of a principal components analysis of the module's gene expression data [32]. The summary expression profile explained 57% of the variance the module's gene expression matrix.

Genome-wide genotyping was carried out on whole blood samples for 2,442 individuals participating in the 2001 follow-up study of the YFS as previously described [25]. Sample and genotype quality control was performed for these 2,442 individuals. Briefly, DNA was extracted and genotyped on a custom 670K Illumina BeadChip array sharing 562,643 SNPs with the Illumina 610 BeadChip array. The custom array removed poorly performing SNPs from the 610 array and improved copy number variation coverage [25]. Genotypes were called using the Illuminus genotype calling algorithm [33]. 2 individuals were removed after initial clustering (call rate < 90%) and 54 samples were subsequently removed following Sanger genotyping pipeline quality control (low call rate: < 90%, failing heterozygosity tests, duplicate samples: >98% concordance on pairwise comparison, previously unknown relationship: >70% concordance on pairwise comparison, or failing Sequenom genotype fingerprinting: < 90% concordance for > 10 genotypes). 546,770 SNPs passed quality control. 3 individuals were removed due to low genotyping success (< 95%) and 1 individual was removed for failing sex checks. 51 individuals were excluded due to previous unknown close relation to another sample (pairwise identity by descent pi-hat > 0.2) and 2 individuals were removed due to cryptic relatedness. Missing genotypes and un-typed SNPs were imputed using the 1000 Genomes Phase 1 (v3) reference panel. Imputed and genotyped SNPs were subsequently excluded where the genotype calling probability for any allele < 90%, information score < 0.4, minor allele frequency < 1% or Hardy Weinberg equilibrium P-value < 5×10^{-6}. A combined total of 6,721,082 directly genotyped and imputed SNPs passed quality control.

Module quantitative trait loci (QTLs) were identified for 1,386 individuals with matched genotype and gene expression data in the YFS through a genome-wide scan for SNPs associated with the summary expression profile using the 1.90 beta (version 3.32) software. Individual associations were tested using a linear model of minor allele dosage on neutrophil module summary expression. A SNP was considered a module QTL where $P < 5 \times 10^{-8}$ (genome-wide significance). Models were adjusted for age, sex, and the first two principal components of the genotype data. The module QTL rs13297295 on chromosome 9 was further tested for an association with expression levels *LCN2* using the same model. Rs13297295 was also tested for association with GlycA and CRP in the 1,712 individuals with matched genotype and GlycA or CRP levels.

LCN2 mRNA levels in human heart

We used data in the repository GEO series GSE1145 to investigate the levels of LCN2 in human idiopathic dilated hearts (n=11 control hearts and n=15 idiopathic dilated hearts). We performed a whole-genome analysis using the GEO tools, including false discovery rate (FDR) adjustment for multiple comparisons, to determine whether LCN2 was over-expressed in human idiopathic dilated hearts.

Table S1. Primers and conditions used to validate microarray gene expression results.

Official gene symbol	GenBank Accession #	Primer Sequence (5' → 3')	Concentration	Product length	Annealing temperature
Rat Gapdh	NM_017008.3	F: GGGGCTCTCTGCTCCTCCCTG R: ACGGCCAAATCCGTTCACACCG	200 nM	108 bp	58ºC
Rat Lcn2	NM_130741.1	F: GGGCTGTCCGATGAACTGAA R: CATTGGTCGGTGGGAACAGA	200 nM	98 bp	58ºC
Human ACTB	NM_001101	F: CGCGAGAAGATGACCCAGAT R: GAGTCCATCACGATGCCAGT	200 nM	119 bp	66 ºC
Human LCN2	NM_005564.3	F: CTACGGGAGAACCAAGGAGC R: CACTGGTCGATTGGGACAGG	200 nM	114 bp	66ºC
Sequencing primers					
Fragment 1	NM_130741.1	F: GGGAGTTTGAGGCTACCTGG R: ATATTGTGCTTCCCTCCCCG	500 nM	1144 bp	55ºC
Fragment 2	NM_130741.1	F: AGGTCAGGAGCAGCAAACAG R: TACTAGGTCCGATGTGTGCC	500 nM	1339 bp	55ºC
Fragment 3	NM_130741.1	F: TCAACAGGATGTGCTGGCAA R: CAGGGTTTCACCTGACGAGG	200 nM	984 bp	58ºC
Fragment 4	NM_130741.1	F: TGCGGTCCAGAAAGAAAGACA R: GACACCCTTCTCCCAGCAAC	200 nM	909 bp	58ºC
Fragment 5	NM_130741.1	F: AATGGACAGGACTCGGGGAA R: TCGCTCCTTCAGTTCATCGG	200 nM	976 bp	58ºC
Fragment 6	NM_130741.1	F: ACTTATGGAGTGTCCTGCGG R: AACACAGGTGGATGGGGAGA	200 nM	950 bp	58ºC
Fragment 7	NM_130741.1	F: CAAGTCTGAGGGTTCGTTTGT R: ACACAGGTGGATGGGGAGA	200 nM	982 bp	58ºC
Fragment 8	NM_130741.1	F: TGTCTGCCGCTCCATCTTTC R: ACCTTCCTGGCCCTAGACAT	200 nM	987 bp	58ºC

*F: forward primer, R: reverse primer, bp: base pairs.

Table S2. RNA-sequencing alignment characteristics of individual sample.

Sample Name	Species	Treatment	Paired Reads	Data Yield (bp)	# Mapped	% Mapped	Correctly paired	# Indels
LCN2_KO_1	mouse	Lcn2 knockout	14,884,071	2.98 Gb	11,954,145	80.3	9,773,674	46,999
LCN2_KO_2	mouse	Lcn2 knockout	18,268,306	3.65 Gb	15,479,156	84.7	12,730,249	61,344
LCN2_KO_4	mouse	Lcn2 knockout	18,081,296	3.62 Gb	15,286,738	84.5	12,666,558	60,985
WT_7	mouse	Wild-type	18,478,701	3.70 Gb	14,802,202	80.1	12,280,683	62,887
WT_8	mouse	Wild-type	20,477,226	4.10 Gb	17,082,133	83.4	13,926,290	65,430
WT_9	mouse	Wild-type	19,197,759	3.84 Gb	15,633,393	81.4	12,863,795	59,517
P_1	rat	Empty plasmid	18,079,037	3.62 Gb	16,643,663	92.1	13,676,516	120,877
P_2	rat	Empty plasmid	18,570,379	3.71 Gb	17,095,842	92.1	13,966,919	127,350
P_3	rat	Empty plasmid	16,296,670	3.26 Gb	14,986,199	92.0	12,217,148	110,047
L_1	rat	Lcn2 plasmid	17,256,951	3.45 Gb	15,898,212	92.1	13,017,963	117,624
L_2	rat	Lcn2 plasmid	16,652,741	3.33 Gb	15,343,993	92.1	12,576,273	113,638
L_3	rat	Lcn2 plasmid	17,646,480	3.53 Gb	16,252,059	92.1	13,287,420	117,522
Total			**213,889,617**	**42.79 Gb**				

Table S3. Characteristics of the participants in the type 2 diabetes cohort.

Characteristic	Subjects without LVH (n=84)	Subjects with LVH (n=30)	*P*-value		
Age (years)	61.2 ± 9.6	65.6 ± 10.5	**0.039**		
Male sex, n (%)	56 (67%)	14 (47%)	0.08		
BMI (kg/m^2)	31.5 ± 6.6	31.9 ± 4.9	0.77		
eGFR (ml/min/1.73cm^2)	86.4 ± 19.4	90.9 ± 25.5	0.32		
Lcn2 (ng/ml)*	38.7 [35.2-41.7]	49.1 [39.8-58.5]	**0.017**	[28.6, 45.2]	44.0 [29.8, 61.4]
Systolic BP (mmHg)	141 ± 19	146 ± 18	0.22		
Hypertension, n (%)	71 (85%)	27 (90%)	0.56		
Structure					
Interventricular septum thickness (cm)	0.98 ± 0.16	1.20 ± 0.18	**<0.0001**		
Posterior wall thickness (cm)	0.96 ± 0.16	1.15 ± 0.12	**<0.0001**		
LV end diastolic dimension (cm)	4.8 ± 0.5	5.3 ± 0.6	**<0.0001**		
LV end systolic dimension (cm)	2.8 ± 0.5	3.2 ± 0.6	**0.001**		
Function					
LV ejection fraction (%)	64 ± 9	63 ± 9	0.73		
s´ medial (cm/s)	6.9 ± 1.4	6.6 ± 0.5	0.28		
E (m/s)	0.75 ± 0.20	0.80 ± 0.19	0.16		
A (m/s)	0.81 ± 0.17	0.89 ± 0.18	**0.040**		
E/A ratio	0.93 ± 0.26	0.94 ± 0.31	0.97		
E' (cm/s)	6.8 ± 1.9	5.8 ± 1.7	**0.016**		
E/E' ratio	11.4 ± 3.5	15.2 ± 4.5	**<0.0001**		
DT (ms)	215 ± 52	228 ± 59	0.26		
IVRT (ms)	92 ± 18	92 ± 30	0.97		

Legend: Data presented as mean ± standard deviation and proportions n. *Lcn2 levels shown as the mean [95% CI]. The *P*-values represent the differences in parameters in those without LVH and with LVH. Legend: LVH, left ventricle hypertrophy; BMI, body mass index, eGFR, estimated glomerular filtration rate; Lcn2, lipocalin-2; BP, blood pressure; CI: confidence intervals.

Table S4. Characteristics of individuals from the YFS cohort.

Characteristic	Prevalence in YFS
Mean age (and range) in years	41.8 (34–49)
Number of individuals	2,064
Male sex, n (%)	936 (45%)
BMI (kg/m^2)	26.5 ± 5.1
Body surface area (m^2)	1.9 ± 0.2
GlycA (mmol/L)	1.6 ± 0.2
CRP (mg/L)	1.7 ± 3.2
Triglycerides (mmol/L)	1.4 ± 0.8
LCN2 microarray probe intensity	10.0 ± 0.96
Systolic blood pressure (mmHg)	119 ± 14
Use of antihypertensive therapy, n (%)	197 (10%)
Use of lipid-lowering therapy	75 (4.0%)
Disease events, n (%)	
Prevalent CVD	20 (0.7%)
Prevalent diabetes	35 (1.3%)
Prevalent cancer	40 (1.4%)
Prevalent immunodeficiency	10 (0.4%)
Recent febrile infection	93 (4.6%)
Structure	
Interventricular septum thickness (cm)	0.73 ± 0.09
LV mass (g/m^2)	135 ± 35
Relative wall thickness to LV diameter (%)	28.1 ± 3.8
Function	
Heart rate during echo (beats per minute)	62 ± 10
LV ejection fraction (%)	58.3 ± 3.6
LV cardiac output (L/minute)	4.7 ± 1.3
LV volume during diastole (mL)	131 ± 32
Ratio of LV mass to end diastolic volume	1.04 ± 0.21
E/A ratio (log-scale)	0.41 ± 0.24
E/E' ratio (log-scale)	1.55 ± 0.21
Systolic myocardial velocity (s') (cm/s)	
measured from lateral wall	13.7 ± 3.3
measured from medial wall	11.0 ± 1.9
Isovolumic relaxation time (IVRT) (ms)	
measured from lateral wall	104 ± 22
measured from medial wall	123 ± 25
Mitral E-wave declaration time (DT) (ms)	217 ± 38

Legend: Data presented as mean ± standard deviation and proportions n (%). LV: left ventricle; BMI: body mass index; CRP: C-reactive protein; CVD: cardiovascular disease. Prevalent disease indicates events occurring prior to sample collection while incident disease indicates events occurring after sample collection.

Table S5. Linear regression of LV phenotypes on *LCN2* expression in the YFS. Models were adjusted for age and sex. Effect size indicates standard deviation (SD) change in left ventricular (LV) phenotype per SD increase in *LCN2* expression.

LV Phenotype	Effect size	95% confidence interval	*P*–value
LV cardiac output	0.11	[0.066, 0.16]	**3×10^{-6}**
Heart rate during echo	0.12	[0.068, 0.17]	**6×10^{-6}**
LV mass	0.084	[0.043, 0.12]	**5×10^{-5}**
E/A ratio	–0.084	[0.043, 0.12]	**5×10^{-4}**
Thickness of interventricular septum	0.077	[0.032, 0.12]	**8×10^{-4}**
LV volume during diastole (end diastolic volume)	0.048	[0.0073, 0.089]	**0.02**
LV isovolumic relaxation time measured from the lateral wall	–0.057	[–0.11, –0.0074]	**0.02**
Ejection fraction	–0.043	[–0.093, 0.0077]	0.10
E/E' ratio	0.034	[–0.016, 0.083]	0.18
Ratio of LV mass to end diastolic volume	0.035	[–0.017, 0.087]	0.19
LV isovolumic relaxation time measured from the medial wall	–0.020	[–0.070, 0.030]	0.43
Systolic myocardial velocity measured from the medial wall	0.020	[–0.030, 0.070]	0.43
Relative LV wall thickness to diameter	0.018	[–0.032, 0.069]	0.47
Systolic myocardial velocity measured from the lateral wall	–0.014	[–0.064, 0.036]	0.59
Mitral E-wave declaration time	–0.00004	[–0.50, 0.050]	1.00

Table S6. Correlation of plasma LCN2 with echocardiogram parameters in the type 2 diabetes cohort.

Structure	Correlation coefficient (Spearman Rho)	*P*-value
Interventricular septum thickness (cm)	0.077	0.418
Posterior wall thickness (cm)	0.165	0.079
LV end diastolic dimension (cm)	0.159	0.091
LV end systolic dimension (cm)	0.146	0.126
Function		
LV ejection fraction (%)	-0.052	0.587
S´ medial (cm/s)	-0.169	0.095
E (m/s)	**-0.258**	**0.006**
A (m/s)	0.081	0.399
E/A ratio	-0.185	0.051
E´ (cm/s)	-0.132	0.162
E/E´ ratio	0.156	0.100
DT (ms)	0.16	0.090
IVRT (ms)	0.038	0.730

Table S7. Transcriptome-wide gene expression array results showing genes differentially expressed in the heart of neonatal HHR (n=8) and NHR (n=8) (only showing genes with *P*-value adjusted by Bonferroni <0.05 and fold difference >2).

Gene Symbol	RefSeq	Bonferroni (*P*-value)	Fold Change	QTL cardiac mass
Akr1b10	NM_001013084	0.00003010000	2.81	
Bphl	NM_001037206	0.00027292800	2.10	Cm34, Cm55
Btnl2	ENSRNOT00000060366	0.00041218200	2.40	
Car4	NM_019174	0.00629238000	–2.06	Cm73, Cm31, Cm78, Cm51, Cm33, Cm44, Cm75
Endog	NM_001034938	0.00000677000	–2.33	Cm43, Cm46, Cm48
Hebp2	NM_001107515	0.00069056300	2.01	
Htr2a	ENSRNOT00000013408	0.00001750000	3.18	
Itgbl1	NM_001017505	0.00005030000	2.58	
Lcn2	ENSRNOT00000018776	0.00000000007	5.02	Cm10, Cm43, Cm46, Cm48
LOC100270669	NM_001144957	0.00348216000	–2.08	Cm29, Cm49
Med22	NM_001077679	0.00000000009	3.07	
Nt5c3a	ENSRNOT00000058703	0.00020376200	2.59	
Pex3	ENSRNOT00000021524	0.00005840000	2.36	
Pop5	NM_001105752	0.01728910000	–2.41	Cm5, Cm72, Cm45, Cm76
RGD1309362	BC098065	0.00349021000	2.29	
RGD1561200	BC160898	0.00000009720	4.47	
Serhl2	NM_001130579	0.00000092500	2.28	Cm27
Trpm8	NM_134371	0.00004230000	–2.79	Cm21, Cm53
Vnn1	NM_001025623	0.00002730000	2.03	
Wdr46	NM_212491	0.00000164000	2.54	
Zfp347	NM_133390	0.00934935000	2.43	

Positive values indicate higher expression in the HHR, and negative values indicate higher expression in the NHR.
Legend: QTL, quantitative trait locus.

Table S8. Gene ontology analysis with all genes differentially expressed with Bonferroni-adjusted *P*-value <0.05.

Function	Type	Enrichment Score	Enrichment *P*-value
cell-cell adhesion	biological process	10.51	0.00003
antigen processing and presentation	biological process	9.36	0.00009
antigen processing and presentation of exogenous peptide antigen via MHC class II	biological process	8.09	0.00031
cell surface	cellular component	7.73	0.00044
mitochondrion	cellular component	7.58	0.00051
intracellular membrane-bounded organelle	cellular component	7.44	0.00059
myosin heavy chain binding	molecular function	7.33	0.00066
response to interferon-alpha	biological process	6.83	0.00109
membrane	cellular component	6.70	0.00123
neuromuscular process	biological process	6.62	0.00134
retinol metabolic process	biological process	6.62	0.00134
retinal dehydrogenase activity	molecular function	6.10	0.00225
LRR domain binding	molecular function	6.10	0.00225
synaptic transmission, glutamatergic	biological process	5.87	0.00281
homotypic cell-cell adhesion	biological process	5.82	0.00298
secretion by cell	biological process	5.82	0.00298
cardiac right ventricle morphogenesis	biological process	5.57	0.00380
heterotrimeric G-protein complex	cellular component	5.38	0.00459
adherens junction	cellular component	5.38	0.00459
NADPH binding	molecular function	5.36	0.00472
spectrin binding	molecular function	5.36	0.00472
water channel activity	molecular function	5.36	0.00472
plasma membrane	cellular component	5.33	0.00484
heparin binding	molecular function	5.32	0.00492
positive regulation of cell death	biological process	5.21	0.00545

positive thymic T cell selection	biological process	5.16	0.00573
generation of precursor metabolites and energy	biological process	5.16	0.00573
multicellular organismal response to stress	biological process	5.16	0.00573
response to cold	biological process	5.05	0.00640
MHC class II protein complex	cellular component	4.99	0.00683
lysosome	cellular component	4.86	0.00773
cell adhesion molecule binding	molecular function	4.83	0.00801
chaperone mediated protein folding requiring cofactor	biological process	4.83	0.00801
fascia adherens	cellular component	4.83	0.00801
dorsal/ventral neural tube patterning	biological process	4.54	0.01064
myoblast differentiation	biological process	4.54	0.01064
water transport	biological process	4.54	0.01064
laminin binding	molecular function	4.42	0.01208
anterior/posterior axis specification	biological process	4.42	0.01208
positive regulation of apoptotic process	biological process	4.38	0.01251
apoptotic process	biological process	4.36	0.01281
olfactory bulb development	biological process	4.30	0.01359
fibroblast growth factor receptor binding	molecular function	4.30	0.01359
SNAP receptor activity	molecular function	4.30	0.01359
immune response	biological process	4.28	0.01385
cytoplasmic membrane-bounded vesicle	cellular component	4.26	0.01410
innate immune response	biological process	4.19	0.01520
structural constituent of muscle	molecular function	4.08	0.01686
response to drug	biological process	4.03	0.01782
protein homotetramerization	biological process	3.99	0.01844
protein homotrimerization	biological process	3.98	0.01860
positive regulation of calcium-mediated signalling	biological process	3.98	0.01860
positive regulation of cardiac muscle cell proliferation	biological process	3.98	0.01860

amino acid transmembrane transporter activity	molecular function	3.98	0.01860
protein sumoylation	biological process	3.98	0.01860
trans-Golgi network	cellular component	3.97	0.01883
blood vessel development	biological process	3.94	0.01937
oxidation-reduction process	biological process	3.91	0.02001
cell-cell junction	cellular component	3.87	0.02083
basolateral plasma membrane	cellular component	3.86	0.02100
cytoplasm	cellular component	3.83	0.02170
positive regulation of smooth muscle cell proliferation	biological process	3.76	0.02338
integrin complex	cellular component	3.72	0.02426
negative regulation of fibroblast proliferation	biological process	3.72	0.02426
eukaryotic cell surface binding	molecular function	3.56	0.02838
tubulin binding	molecular function	3.56	0.02838
lysosome organization	biological process	3.56	0.02838
RNA polymerase II transcription cofactor activity	molecular function	3.49	0.03053
ATPase activity, coupled to transmembrane movement of substances	molecular function	3.49	0.03053
positive regulation of BMP signalling pathway	biological process	3.49	0.03053
positive regulation of interleukin-4 biosynthetic process	biological process	3.46	0.03136
antigen processing and presentation, exogenous lipid antigen via MHC class Ib	biological process	3.46	0.03136
medium-chain fatty acid transport	biological process	3.46	0.03136
eye photoreceptor cell differentiation	biological process	3.46	0.03136
NADP-retinol dehydrogenase activity	molecular function	3.46	0.03136
thermoception	biological process	3.46	0.03136
5-phosphoribose 1-diphosphate biosynthetic process	biological process	3.46	0.03136
glycogen phosphorylase activity	molecular function	3.46	0.03136

mRNA cis splicing, via spliceosome	biological process	3.46	0.03136
platelet activating factor biosynthetic process	biological process	3.46	0.03136
myosin filament assembly	biological process	3.46	0.03136
ferroxidase activity	molecular function	3.46	0.03136
coated vesicle	cellular component	3.46	0.03136
chemical homeostasis	biological process	3.46	0.03136
protein localization to adherens junction	biological process	3.46	0.03136
photoreceptor cell outer segment organization	biological process	3.46	0.03136
death domain binding	molecular function	3.46	0.03136
thiol oxidase activity	molecular function	3.46	0.03136
cuticular plate	cellular component	3.46	0.03136
pulmonary myocardium development	biological process	3.46	0.03136
antigen processing and presentation of exogenous peptide antigen via MHC class I	biological process	3.46	0.03136
optic cup morphogenesis involved in camera-type eye development	biological process	3.46	0.03136
double-stranded RNA adenosine deaminase activity	molecular function	3.46	0.03136
supraspliceosomal complex	cellular component	3.46	0.03136
ubiquitin homeostasis	biological process	3.46	0.03136
tangential migration from the subventricular zone to the olfactory bulb	biological process	3.46	0.03136
positive regulation of dopamine receptor signalling pathway	biological process	3.46	0.03136
specification of organ position	biological process	3.46	0.03136
blood vessel endothelial cell proliferation involved in sprouting angiogenesis	biological process	3.46	0.03136
BMP signalling pathway involved in heart induction	biological process	3.46	0.03136
deltoid tuberosity development	biological process	3.46	0.03136
mesodermal cell differentiation	biological process	3.46	0.03136

cloacal septation	biological process	3.46	0.03136
regulation of pathway-restricted SMAD protein phosphorylation	biological process	3.46	0.03136
trachea formation	biological process	3.46	0.03136
bud elongation involved in lung branching	biological process	3.46	0.03136
regulation of cartilage development	biological process	3.46	0.03136
mesenchymal cell proliferation involved in ureteric bud development	biological process	3.46	0.03136
ureter smooth muscle cell differentiation	biological process	3.46	0.03136
plasma cell differentiation	biological process	3.46	0.03136
glycosphingolipid biosynthetic process	biological process	3.46	0.03136
connexin binding	molecular function	3.46	0.03136
nucleolar ribonuclease P complex	cellular component	3.46	0.03136
homocysteine S-methyltransferase activity	molecular function	3.46	0.03136
inorganic diphosphate transport	biological process	3.46	0.03136
sequestering of triglyceride	biological process	3.46	0.03136
NADH pyrophosphatase activity	molecular function	3.46	0.03136
response to iron(III) ion	biological process	3.46	0.03136
response to anoxia	biological process	3.46	0.03136
virus-infected cell apoptotic process	biological process	3.46	0.03136
folic acid transporter activity	molecular function	3.46	0.03136
creatine kinase activity	molecular function	3.46	0.03136
regulation of mast cell activation	biological process	3.46	0.03136
regulation of Fc receptor mediated stimulatory signalling pathway	biological process	3.46	0.03136
ganglioside catabolic process	biological process	3.46	0.03136
oligosaccharide catabolic process	biological process	3.46	0.03136
glycerol channel activity	molecular function	3.46	0.03136
forebrain cell migration	biological process	3.46	0.03136
negative regulation of lymphocyte activation	biological process	3.46	0.03136

axon midline choice point recognition	biological process	3.46	0.03136
olfactory bulb interneuron development	biological process	3.46	0.03136
Roundabout signalling pathway	biological process	3.46	0.03136
regulation of epidermal growth factor receptor signalling pathway	biological process	3.46	0.03136
localization within membrane	biological process	3.46	0.03136
low-density lipoprotein particle mediated signalling	biological process	3.46	0.03136
alanine-tRNA ligase activity	molecular function	3.46	0.03136
alanyl-tRNA aminoacylation	biological process	3.46	0.03136
transferrin transport	biological process	3.46	0.03136
endocardial cushion to mesenchymal transition involved in heart valve formation	biological process	3.46	0.03136
ascending aorta morphogenesis	biological process	3.46	0.03136
microsatellite binding	molecular function	3.46	0.03136
arterial endothelial cell differentiation	biological process	3.46	0.03136
cardiac vascular smooth muscle cell development	biological process	3.46	0.03136
protease binding	molecular function	3.46	0.03138
activation of MAPKK activity	biological process	3.42	0.03275
neuromuscular junction development	biological process	3.35	0.03503
response to retinoic acid	biological process	3.35	0.03520
regulation of cell shape	biological process	3.24	0.03925
cellular response to hydrogen peroxide	biological process	3.22	0.03977
protein kinase B signalling cascade	biological process	3.22	0.03977
cell adhesion	biological process	3.20	0.04081
positive regulation of cell projection organization	biological process	3.18	0.04159
T cell receptor binding	molecular function	3.18	0.04159
positive regulation of NK T cell activation	biological process	3.18	0.04159
neurotransmitter metabolic process	biological process	3.18	0.04159
smooth muscle cell migration	biological process	3.18	0.04159
positive regulation of ovulation	biological process	3.18	0.04159

peroxisome membrane biogenesis	biological process	3.18	0.04159
vitamin binding	molecular function	3.18	0.04159
biotin binding	molecular function	3.18	0.04159
rhythmic synaptic transmission	biological process	3.18	0.04159
sphingosine metabolic process	biological process	3.18	0.04159
regulation of striated muscle contraction	biological process	3.18	0.04159
glycosaminoglycan catabolic process	biological process	3.18	0.04159
morphogenesis of a polarized epithelium	biological process	3.18	0.04159
phospholipid dephosphorylation	biological process	3.18	0.04159
AP-1 adaptor complex	cellular component	3.18	0.04159
protein thiol-disulfide exchange	biological process	3.18	0.04159
dichotomous subdivision of terminal units involved in salivary gland branching	biological process	3.18	0.04159
epsilon DNA polymerase complex	cellular component	3.18	0.04159
phospholipid transporter activity	molecular function	3.18	0.04159
telomerase activity	molecular function	3.18	0.04159
telomere maintenance via recombination	biological process	3.18	0.04159
ferric-chelate reductase activity	molecular function	3.18	0.04159
fat pad development	biological process	3.18	0.04159
female meiosis I	biological process	3.18	0.04159
exploration behaviour	biological process	3.18	0.04159
intracellular distribution of mitochondria	biological process	3.18	0.04159
negative regulation of dendritic spine morphogenesis	biological process	3.18	0.04159
negative regulation of inclusion body assembly	biological process	3.18	0.04159
telencephalon regionalization	biological process	3.18	0.04159
negative regulation of T cell differentiation in thymus	biological process	3.18	0.04159
negative regulation of immature T cell proliferation in thymus	biological process	3.18	0.04159

tendon cell differentiation	biological process	3.18	0.04159
trachea development	biological process	3.18	0.04159
prostate gland morphogenesis	biological process	3.18	0.04159
negative regulation of prostatic bud formation	biological process	3.18	0.04159
regulation of morphogenesis of a branching structure	biological process	3.18	0.04159
negative regulation of thymocyte apoptotic process	biological process	3.18	0.04159
negative regulation of branching involved in ureteric bud morphogenesis	biological process	3.18	0.04159
epithelial structure maintenance	biological process	3.18	0.04159
cardiac muscle fibre development	biological process	3.18	0.04159
transepithelial transport	biological process	3.18	0.04159
nucleotide diphosphatase activity	molecular function	3.18	0.04159
nucleoside-triphosphate diphosphatase activity	molecular function	3.18	0.04159
nucleoside triphosphate catabolic process	biological process	3.18	0.04159
folic acid transport	biological process	3.18	0.04159
water transmembrane transporter activity	molecular function	3.18	0.04159
response to interferon-beta	biological process	3.18	0.04159
phosphatidylserine biosynthetic process	biological process	3.18	0.04159
beta-N-acetylhexosaminidase activity	molecular function	3.18	0.04159
selenocysteine incorporation	biological process	3.18	0.04159
negative regulation of chemokine-mediated signalling pathway	biological process	3.18	0.04159
regulation of translational fidelity	biological process	3.18	0.04159
negative regulation of vasodilation	biological process	3.18	0.04159
negative regulation of wound healing	biological process	3.18	0.04159
negative regulation of insulin secretion involved in cellular response to glucose stimulus	biological process	3.18	0.04159
muscular septum morphogenesis	biological process	3.18	0.04159
dorsal aorta morphogenesis	biological process	3.18	0.04159

pulmonary artery morphogenesis	biological process	3.18	0.04159
vascular smooth muscle cell development	biological process	3.18	0.04159
serine-type carboxypeptidase activity	molecular function	3.18	0.04159
centrosome	cellular component	3.17	0.04214
mediator complex	cellular component	3.16	0.04222
ATP hydrolysis coupled proton transport	biological process	3.16	0.04222
peptidyl-tyrosine dephosphorylation	biological process	3.16	0.04222
intercalated disc	cellular component	3.16	0.04222
embryonic hindlimb morphogenesis	biological process	3.16	0.04222
response to bacterium	biological process	3.11	0.04473
positive regulation of proteasomal ubiquitin-dependent protein catabolic process	biological process	3.11	0.04473
odontogenesis	biological process	3.11	0.04473
negative regulation of MAP kinase activity	biological process	3.11	0.04473
adult walking behaviour	biological process	3.05	0.04729
actin cytoskeleton reorganization	biological process	3.05	0.04729
metal ion binding	molecular function	3.04	0.04770
receptor binding	molecular function	3.03	0.04816
sarcolemma	cellular component	3.00	0.04956
cation binding	molecular function	3.00	0.04991
blood vessel remodeling	biological process	3.00	0.04991

Table S9. Gene set enrichment analysis, based on gene ontology, of the gene list for differentially expressed genes between HHR and NHR (P<0.05).

Gene Set	Gene Set Description	Number of Markers	ES	NES	*P*-value	HHR vs NHR
60048	cardiac muscle contraction	30	–0.57	–1.99	<0.001	Down
35335	peptidyl-tyrosine dephosphorylation	38	–0.56	–1.96	<0.001	Down
97110	scaffold protein binding	25	–0.55	–1.93	<0.001	Down
16459	myosin complex	42	–0.60	–1.90	<0.001	Down
30017	sarcomere	26	–0.59	–1.99	<0.001	Down
3774	motor activity	51	–0.53	–1.87	<0.001	Down
55010	ventricular cardiac muscle tissue morphogenesis	26	–0.58	–1.87	<0.001	Down
5089	Rho guanyl-nucleotide exchange factor activity	61	–0.53	–1.84	<0.001	Down
45859	regulation of protein kinase activity	18	–0.67	–1.82	<0.001	Down
35108	limb morphogenesis	24	–0.54	–1.78	<0.001	Down
3777	microtubule motor activity	68	–0.48	–1.78	<0.001	Down
45747	positive regulation of Notch signalling pathway	17	–0.66	–1.77	<0.001	Down
32880	regulation of protein localization	40	0.49	1.81	<0.001	Up
5216	ion channel activity	51	–0.51	–1.79	<0.001	Down
45087	innate immune response	87	0.43	1.80	<0.001	Up
9635	response to herbicide	17	0.59	1.82	<0.001	Up
36094	small molecule binding	17	0.79	1.79	<0.001	Up
42098	T cell proliferation	18	–0.66	–1.75	<0.001	Down
16592	mediator complex	30	0.53	1.78	<0.001	Up
30016	myofibril	46	–0.60	–1.79	<0.001	Down
30506	ankyrin binding	21	–0.70	–1.75	<0.001	Down
6730	one-carbon metabolic process	30	0.55	1.70	<0.001	Up
17134	fibroblast growth factor binding	28	0.61	1.83	<0.001	Up
8146	sulfotransferase activity	30	0.49	1.71	<0.001	Up
10765	positive regulation of sodium ion transport	21	0.54	1.71	<0.001	Up
45471	response to ethanol	139	0.43	1.71	<0.001	Up

15171	amino acid transmembrane transporter activity	20	0.64	1.87	<0.001	Up
5758	mitochondrial intermembrane space	43	0.56	1.72	<0.001	Up
1965	G-protein alpha-subunit binding	22	0.54	1.67	<0.001	Up
16925	protein sumoylation	23	0.52	1.65	<0.001	Up
15807	L-amino acid transport	20	0.58	1.66	<0.001	Up
9636	response to toxin	95	0.43	1.75	<0.001	Up
19233	sensory perception of pain	68	0.42	1.66	<0.001	Up
6164	purine nucleotide biosynthetic process	15	0.68	1.73	<0.001	Up
10862	positive regulation of pathway-restricted SMAD protein phosphorylation	23	0.71	1.73	<0.001	Up
9615	response to virus	100	0.44	1.83	<0.001	Up
6979	response to oxidative stress	126	0.39	1.62	<0.001	Up
5771	multivesicular body	20	0.51	1.61	<0.001	Up
71356	cellular response to tumor necrosis factor	42	0.46	1.61	<0.001	Up
30838	positive regulation of actin filament polymerization	32	0.45	1.57	<0.001	Up
9725	response to hormone stimulus	100	0.38	1.54	<0.001	Up
6103	2-oxoglutarate metabolic process	16	0.71	1.57	<0.001	Up
34446	substrate adhesion-dependent cell spreading	23	0.54	1.63	<0.001	Up
118	histone deacetylase complex	24	–0.47	–1.71	<0.001	Down
70207	protein homotrimerization	21	0.48	1.55	<0.001	Up
35265	organ growth	16	–0.56	–1.69	<0.001	Down
10165	response to X-ray	20	0.49	1.55	<0.001	Up
15908	fatty acid transport	18	0.56	1.57	<0.001	Up
7031	peroxisome organization	21	0.57	1.59	<0.001	Up
9966	regulation of signal transduction	26	–0.45	–1.68	<0.001	Down
7266	Rho protein signal transduction	31	0.42	1.63	<0.001	Up
5516	calmodulin binding	119	–0.39	–1.66	<0.001	Down
1968	fibronectin binding	19	0.66	1.83	<0.001	Up
30182	neuron differentiation	109	0.34	1.50	<0.001	Up

16874	ligase activity	39	0.46	1.47	<0.001	Up
1104	RNA polymerase II transcription cofactor activity	25	0.56	1.89	<0.001	Up
187	activation of MAPK activity	64	–0.39	–1.63	<0.001	Down
21549	cerebellum development	41	–0.41	–1.60	<0.001	Down
43292	contractile fibre	17	–0.61	–1.63	<0.001	Down
10524	positive regulation of calcium ion transport into cytosol	15	–0.57	–1.62	<0.001	Down
3333	amino acid transmembrane transport	34	0.65	1.93	<0.001	Up
48513	organ development	16	–0.65	–1.62	<0.001	Down
43274	phospholipase binding	16	–0.52	–1.55	<0.001	Down
7050	cell cycle arrest	75	–0.40	–1.58	<0.001	Down
10628	positive regulation of gene expression	163	0.33	1.39	<0.001	Up
45597	positive regulation of cell differentiation	36	0.41	1.37	<0.001	Up
5080	protein kinase C binding	42	–0.44	–1.56	<0.001	Down
8289	lipid binding	94	0.33	1.38	<0.001	Up
7528	neuromuscular junction development	28	–0.49	–1.53	<0.001	Down
5604	basement membrane	77	–0.39	–1.50	<0.001	Down
42391	regulation of membrane potential	60	–0.39	–1.51	<0.001	Down
51091	positive regulation of sequence-specific DNA binding transcription factor activity	75	–0.42	–1.49	<0.001	Down
30667	secretory granule membrane	17	–0.50	–1.48	<0.001	Down
50852	T cell receptor signalling pathway	32	–0.40	–1.46	<0.001	Down
48485	sympathetic nervous system development	20	–0.51	–1.46	<0.001	Down
8060	ARF GTPase activator activity	22	–0.50	–1.46	<0.001	Down
51924	regulation of calcium ion transport	33	–0.40	–1.38	<0.001	Down
10212	response to ionizing radiation	47	0.36	1.39	0.018	Up
2020	protease binding	67	0.41	1.62	0.019	Up
5215	transporter activity	133	0.36	1.51	0.019	Up
43200	response to amino acid stimulus	47	0.47	1.59	0.019	Up
45861	negative regulation of proteolysis	20	0.53	1.62	0.019	Up

31667	response to nutrient levels	64	0.41	1.58	0.019	Up
9617	response to bacterium	32	0.46	1.53	0.019	Up
1937	negative regulation of endothelial cell proliferation	25	–0.45	–1.55	0.019	Down
7219	Notch signalling pathway	59	–0.34	–1.43	0.019	Down
33077	T cell differentiation in thymus	31	0.49	1.45	0.020	Up
70301	cellular response to hydrogen peroxide	30	0.50	1.70	0.020	Up
42573	retinoic acid metabolic process	16	0.58	1.70	0.020	Up
50776	regulation of immune response	20	0.47	1.55	0.020	Up
15450	P-P-bond-hydrolysis-driven protein transmembrane transporter activity	17	0.68	1.68	0.020	Up
46686	response to cadmium ion	30	0.49	1.62	0.020	Up
6829	zinc ion transport	18	0.63	1.58	0.020	Up
5671	Ada2/Gcn5/Ada3 transcription activator complex	15	0.55	1.56	0.020	Up
7610	behaviour	31	0.48	1.60	0.021	Up
8301	DNA binding, bending	58	–0.56	–1.70	0.021	Down
19003	GDP binding	33	0.67	1.58	0.021	Up
86091	regulation of heart rate by cardiac conduction	16	–0.58	–1.66	0.021	Down
7417	central nervous system development	71	0.34	1.36	0.021	Up
16023	cytoplasmic membrane-bounded vesicle	89	–0.34	–1.43	0.021	Down
45669	positive regulation of osteoblast differentiation	52	0.44	1.54	0.021	Up
48546	digestive tract morphogenesis	17	0.57	1.51	0.021	Up
51287	NAD binding	80	0.66	1.74	0.022	Up
35255	ionotropic glutamate receptor binding	22	0.53	1.54	0.022	Up
1501	skeletal system development	73	0.36	1.46	0.022	Up
16581	NuRD complex	19	–0.47	–1.51	0.022	Down
48812	neuron projection morphogenesis	39	0.40	1.34	0.022	Up
8016	regulation of heart contraction	22	–0.42	–1.45	0.022	Down
6096	glycolysis	77	0.67	1.73	0.022	Up
51015	actin filament binding	68	–0.46	–1.68	0.022	Down

71805	potassium ion transmembrane transport	18	–0.58	–1.59	0.022	Down
42995	cell projection	68	0.36	1.39	0.022	Up
8092	cytoskeletal protein binding	50	–0.41	–1.52	0.022	Down
5506	iron ion binding	189	0.37	1.58	0.023	Up
1836	release of cytochrome c from mitochondria	21	0.60	1.55	0.023	Up
46933	hydrogen ion transporting ATP synthase activity, rotational mechanism	16	0.60	1.63	0.023	Up
3007	heart morphogenesis	37	–0.44	–1.56	0.023	Down
6897	endocytosis	87	–0.38	–1.55	0.023	Down
6099	tricarboxylic acid cycle	23	0.63	1.55	0.023	Up
1078	RNA polymerase II core promoter proximal region sequence-specific DNA binding transcription factor activity involved in negative regulation of transcription	30	–0.41	–1.41	0.023	Down
21772	olfactory bulb development	16	–0.62	–1.74	0.024	Down
70588	calcium ion transmembrane transport	50	–0.47	–1.71	0.024	Down
6816	calcium ion transport	88	–0.42	–1.56	0.024	Down
4190	aspartic-type endopeptidase activity	18	0.54	1.46	0.024	Up
35023	regulation of Rho protein signal transduction	59	–0.49	–1.69	0.025	Down
32874	positive regulation of stress-activated MAPK cascade	18	–0.60	–1.76	0.026	Down
16323	basolateral plasma membrane	154	–0.39	–1.57	0.026	Down
3779	actin binding	220	–0.39	–1.52	0.028	Down
1822	kidney development	116	0.30	1.32	0.036	Up
43499	eukaryotic cell surface binding	26	0.55	1.69	0.036	Up
10243	response to organic nitrogen	63	0.40	1.52	0.036	Up
16787	hydrolase activity	122	0.41	1.68	0.037	Up
14823	response to activity	48	0.40	1.46	0.037	Up
46328	regulation of JNK cascade	17	–0.47	–1.48	0.037	Down
30279	negative regulation of ossification	18	0.55	1.55	0.038	Up

70371	ERK1 and ERK2 cascade	21	0.49	1.55	0.038	Up
30100	regulation of endocytosis	20	0.48	1.45	0.038	Up
1516	prostaglandin biosynthetic process	16	0.46	1.45	0.038	Up
45454	cell redox homeostasis	52	0.41	1.49	0.039	Up
55114	oxidation-reduction process	259	0.37	1.57	0.040	Up
45987	positive regulation of smooth muscle contraction	18	0.53	1.52	0.040	Up
45907	positive regulation of vasoconstriction	28	0.45	1.49	0.040	Up
15459	potassium channel regulator activity	21	0.49	1.49	0.040	Up
51219	phosphoprotein binding	41	–0.40	–1.53	0.040	Down
6633	fatty acid biosynthetic process	42	–0.40	–1.46	0.040	Down
1958	endochondral ossification	23	0.49	1.58	0.041	Up
1974	blood vessel remodeling	35	0.45	1.48	0.041	Up
4221	ubiquitin thiolesterase activity	64	–0.41	–1.54	0.041	Down
5525	GTP binding	355	0.44	1.57	0.042	Up
8307	structural constituent of muscle	18	–0.63	–1.66	0.042	Down
60395	SMAD protein signal transduction	18	0.56	1.51	0.042	Up
43484	regulation of RNA splicing	21	–0.47	–1.57	0.042	Down
5070	SH3/SH2 adaptor activity	17	–0.56	–1.54	0.042	Down
30286	dynein complex	22	–0.53	–1.55	0.042	Down
30217	T cell differentiation	33	–0.43	–1.54	0.042	Down
1656	metanephros development	33	0.40	1.38	0.042	Up
60359	response to ammonium ion	35	0.85	1.68	0.043	Up
1657	ureteric bud development	44	0.45	1.54	0.043	Up
4365	glyceraldehyde-3-phosphate dehydrogenase (NAD+) (phosphorylating) activity	34	0.84	1.63	0.043	Up
71333	cellular response to glucose stimulus	30	0.42	1.46	0.043	Up
51056	regulation of small GTPase mediated signal transduction	59	–0.49	–1.61	0.043	Down
32266	phosphatidylinositol-3-phosphate binding	17	–0.51	–1.60	0.043	Down
30889	negative regulation of B cell proliferation	15	0.53	1.41	0.043	Up

7257	activation of JUN kinase activity	25	–0.45	–1.52	0.043	Down
51018	protein kinase A binding	16	–0.51	–1.42	0.043	Down
15991	ATP hydrolysis coupled proton transport	34	0.48	1.61	0.043	Up
50821	protein stabilization	99	0.56	1.63	0.043	Up
31397	negative regulation of protein ubiquitination	24	0.53	1.51	0.043	Up
2027	regulation of heart rate	20	–0.56	–1.57	0.043	Down
32312	regulation of ARF GTPase activity	21	–0.49	–1.47	0.043	Down
17048	Rho GTPase binding	24	–0.58	–1.71	0.044	Down
42383	sarcolemma	81	–0.41	–1.55	0.044	Down
71889	14-3-3 protein binding	17	–0.59	–1.58	0.044	Down
7628	adult walking behaviour	34	–0.37	–1.38	0.044	Down
35267	NuA4 histone acetyltransferase complex	16	–0.55	–1.70	0.045	Down
30032	lamellipodium assembly	25	0.51	1.54	0.045	Up
10039	response to iron ion	21	0.58	1.50	0.045	Up
5543	phospholipid binding	284	–0.36	–1.52	0.045	Down
4725	protein tyrosine phosphatase activity	96	–0.36	–1.46	0.045	Down
45765	regulation of angiogenesis	17	0.60	1.45	0.047	Up
31175	neuron projection development	105	–0.33	–1.37	0.047	Down
6874	cellular calcium ion homeostasis	69	–0.38	–1.43	0.048	Down
48037	cofactor binding	18	0.42	1.45	0.049	Up

Legend: ES; enrichment score; NES, normalized enrichment score.

Table S10. Genes differentially expressed between Lcn2-knockout compared to wild-type mice identified by RNA-sequencing (n=3/group). Here shown only genes with false discovery rate (FDR) q<0.05.

GeneID	logFC	*P*-value	q-value
Hspa1a	–2.15	1.13E-10	1.00E-06
Nr4a1	–2.53	1.52E-10	1.00E-06
Hspa1b	–2.50	2.35E-09	1.03E-05
Zbtb16	2.93	7.95E-09	2.63E-05
Hamp	–4.70	1.78E-07	0.00047
Hif3a	2.77	8.97E-07	0.0018
Myl4	–4.09	9.52E-07	0.0018
Adipoq	–4.90	2.71E-06	0.0045
Lcn2	–2.25	1.06E-05	0.0155
Slc4a8	2.16	1.47E-05	0.0195
Fkbp5	1.38	1.72E-05	0.0195
Cfd	–3.38	1.78E-05	0.0195
Sln	–4.29	2.50E-05	0.0255
Pdk4	1.68	3.17E-05	0.0299
Serpine1	1.11	4.53E-05	0.0399
Map3k6	1.31	5.30E-05	0.0437

*logFC: logarithmic fold change.

Table S11. Gene set enrichment analysis with differentially expressed genes between Lcn2-knockout compared to wild-type mice.

Category	Term	Count	Total	%	Involved Genes	Fold Enrichment	*P*-Value
KEGG_PATHWAY	mmu04510: Focal adhesion	31	198	15.7	*MYL7, XIAP, ACTG1, ARHGAP5, COL6A6, COMP, ITGB6, PPP1R12A, PDGFD, EGF, PIK3R1, FN1, COL4A4, COL4A2, COL4A1, FLT1, ROCK2, ITGA1, ITGA2, HGF, FLNB, COL5A1, KDR, LAMA2, LAMA3, LAMA5, ITGA8, PDGFRA, LAMC1, MYLK, ITGA2B*	4.36	7.98E-12
KEGG_PATHWAY	mmu04512: ECM-receptor interaction	17	83	20.5	*COL4A4, COL4A2, COL4A1, ITGA1, ITGA2, COL5A1, HMMR, LAMA2, LAMA3, COL6A6, LAMA5, COMP, ITGA8, ITGB6, LAMC1, ITGA2B, FN1*	5.70	2.45E-08
KEGG_PATHWAY	mmu05222: Small cell lung cancer	14	85	16.5	*COL4A4, COL4A2, COL4A1, XIAP, ITGA2, CCNE2, LAMA2, LAMA3, CDKN2B, LAMA5, LAMC1, PIK3R1, FN1, ITGA2B*	4.59	8.06E-06
KEGG_PATHWAY	mmu05200: Pathways in cancer	29	323	9.0	*XIAP, FOXO1, FGF12, ZBTB16, CCNE2, CDKN2B, TPR, EGF, PIK3R1, FN1, APC, COL4A4, COL4A2, COL4A1, EPAS1, RUNX1T1, ITGA2, BRCA2, HGF, STAT1, CTNNA3, WNT2B, LAMA2, CBLC, LAMA3, LAMA5, PDGFRA, LAMC1, ITGA2B*	2.50	9.08E-06
KEGG_PATHWAY	mmu04810: Regulation of actin cytoskeleton	20	217	9.2	*MYL7, ROCK2, ITGAE, SSH2, ITGA1, ITGA2, FGF12, ACTG1, ITGA8, ITGB6, PPP1R12A, PDGFRA,*	2.57	2.44E-04

					PDGFD, EGF, DIAP2, PIK3R1, MYLK, ITGA2B, APC, FN1		
KEGG_PATHWAY	mmu05412: Arrhythmogenic right ventricular cardiomyopathy (ARVC)	11	75	14.7	*LAMA2, ACTG1, DMD, ITGA8, ITGB6, CACNG6, ITGA1, ITGA2, RYR2, CTNNA3, ITGA2B*	4.08	2.96E-04
KEGG_PATHWAY	mmu05410: Hypertrophic cardiomyopathy (HCM)	11	84	13.1	*LAMA2, ACTG1, DMD, ITGA8, ITGB6, CACNG6, ITGA1, ITGA2, RYR2, TTN, ITGA2B*	3.65	7.46E-04
KEGG_PATHWAY	mmu05414: Dilated cardiomyopathy	11	92	12.0	*LAMA2, ACTG1, DMD, ITGA8, ITGB6, CACNG6, ITGA1, ITGA2, RYR2, TTN, ITGA2B*	3.33	0.001
KEGG_PATHWAY	mmu04540: Gap junction	9	86	10.5	*PLCB4, MAP3K2, GUCY1A2, PDGFRA, PDGFD, PRKG1, EGF, ITPR1, ITPR2*	2.91	0.011
KEGG_PATHWAY	mmu04144: Endocytosis	15	202	7.4	*FLT1, ERBB4, PSD3, ASAP1, HSPA1A, EEA1, HSPA1B, KDR, CBLC, RAB11FIP2, TFRC, HSPA2, PDGFRA, H2-T24, EGF, AGAP2*	2.07	0.013
KEGG_PATHWAY	mmu04270: Vascular smooth muscle contraction	10	120	8.3	*PLCB4, ROCK2, MYH11, PPP1R12A, GUCY1A2, ADRA1A, PRKG1, ITPR1, MYLK, ITPR2*	2.32	0.027

Footnote: Count: number of genes from 721 differentially expressed genes (P<0.05) involved in that pathway; %: genes involved/total number of genes in pathway; P-value: modified Fisher exact P-value.

Table S12. Gene set enrichment analysis with the differentially expressed genes between cells transfected with Lcn2 or empty plasmid.

Category	Term	Count	Total	%	Involved genes	Fold Enrichment	*P*-Value
KEGG_PATHWAY	rno05222: Small cell lung cancer	10	83	12.0	*E2F3, PTGS2, ITGA6, BCL2, BCL2L1, RB1, BIRC3, BIRC2, MYC, TRAF4*	4.46	3.43E-04
KEGG_PATHWAY	rno04510: Focal adhesion	13	195	6.7	*CAV1, ROCK2, COL3A1, ITGA11, ITGB5, BIRC3, BIRC2, ITGA6, RASGRF1, BCL2, GSK3B, THBS2, MYLK*	2.47	0.006
KEGG_PATHWAY	rno04110: Cell cycle	10	126	7.9	*E2F3, CCNH, PLK1, GSK3B, BUB1, CDC20, RB1, CDC25C, ABL1, MYC*	2.94	0.006
KEGG_PATHWAY	rno04142: Lysosome	9	117	7.7	*TCIRG1, AP1S2, GUSB, HEXA, LGMN, CTSD, PPT1, FUCA1, MANBA*	2.85	0.013
KEGG_PATHWAY	rno05200: Pathways in cancer	15	317	4.7	*E2F3, FGF7, PTGS2, BCL2L1, RB1, BIRC3, STAT1, BIRC2, FZD6, ITGA6, BCL2, GSK3B, ABL1, MYC, TRAF4*	1.75	0.04
KEGG_PATHWAY	rno00511: Other glycan degradation	3	16	18.8	*HEXA, FUCA1, MANBA*	6.94	0.067
KEGG_PATHWAY	rno05410: Hypertrophic cardiomyopathy (HCM)	6	84	7.1	*ACTC1, ITGA6, ITGA11, ITGB5, CACNG1, TNNI3*	2.64	0.074
KEGG_PATHWAY	rno04114: Oocyte meiosis	7	111	6.3	*REC8, SLK, PLK1, BUB1, CDC20, AURKA, CDC25C*	2.33	0.077
KEGG_PATHWAY	rno05414: Dilated cardiomyopathy	6	90	6.7	*ACTC1, ITGA6, ITGA11, ITGB5, CACNG1, TNNI3*	2.47	0.09

Footnote: Count: number of genes from 529 differentially expressed genes ($P<0.05$) involved in that pathway; %: genes involved/total number of genes in pathway; *P*-value: modified Fisher exact *P*-value.

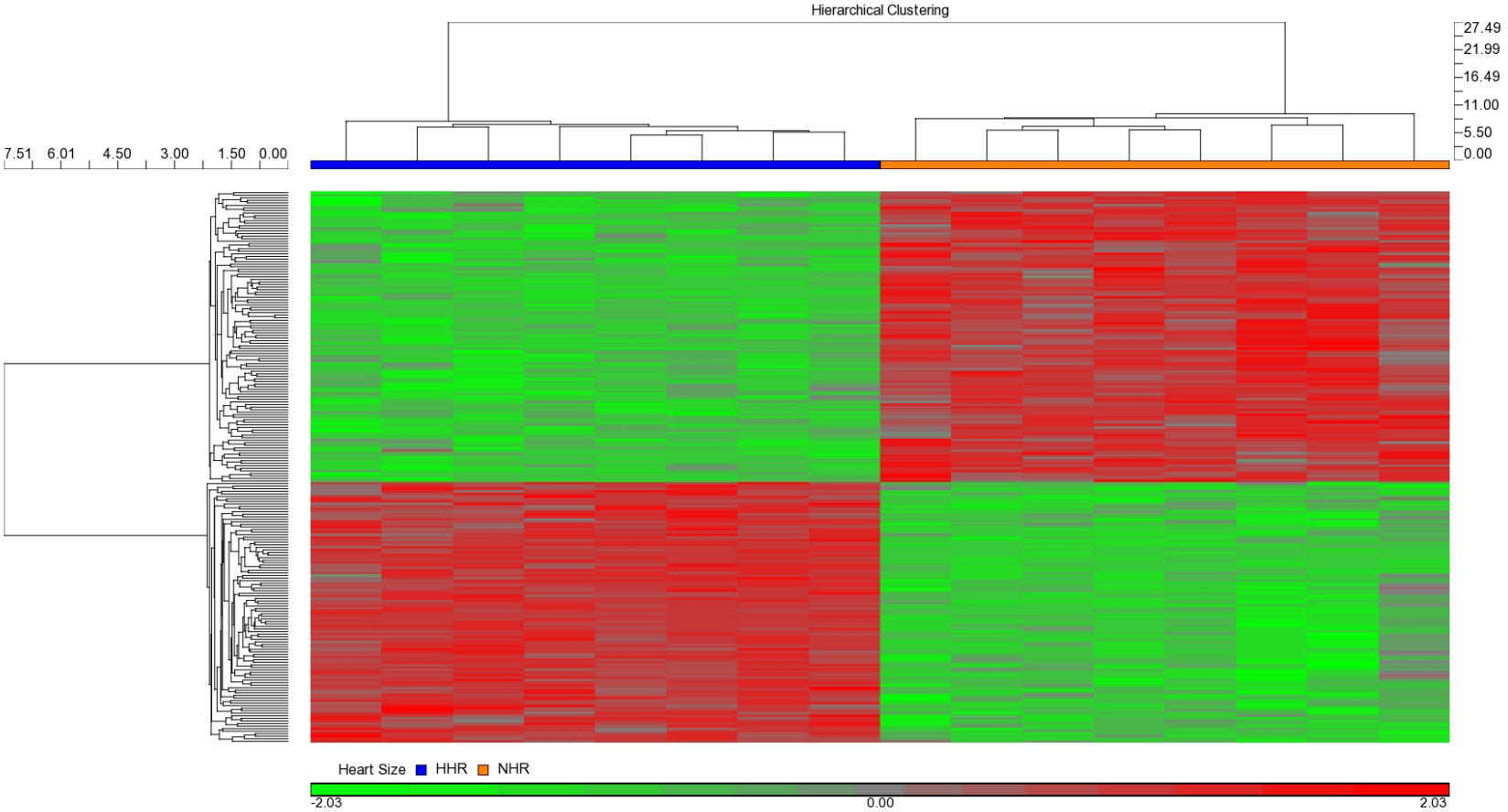

Figure S1. Hierarchical clustering showing that neonatal hypertrophic heart rat (HHR) (blue) and normal heart rat (NHR) (orange) form distinct groups based on gene expression (genes with Bonferroni adjustment <0.05). Numbers on the right are probeset numbers. Red depicts genes up-regulated and green those down-regulated.

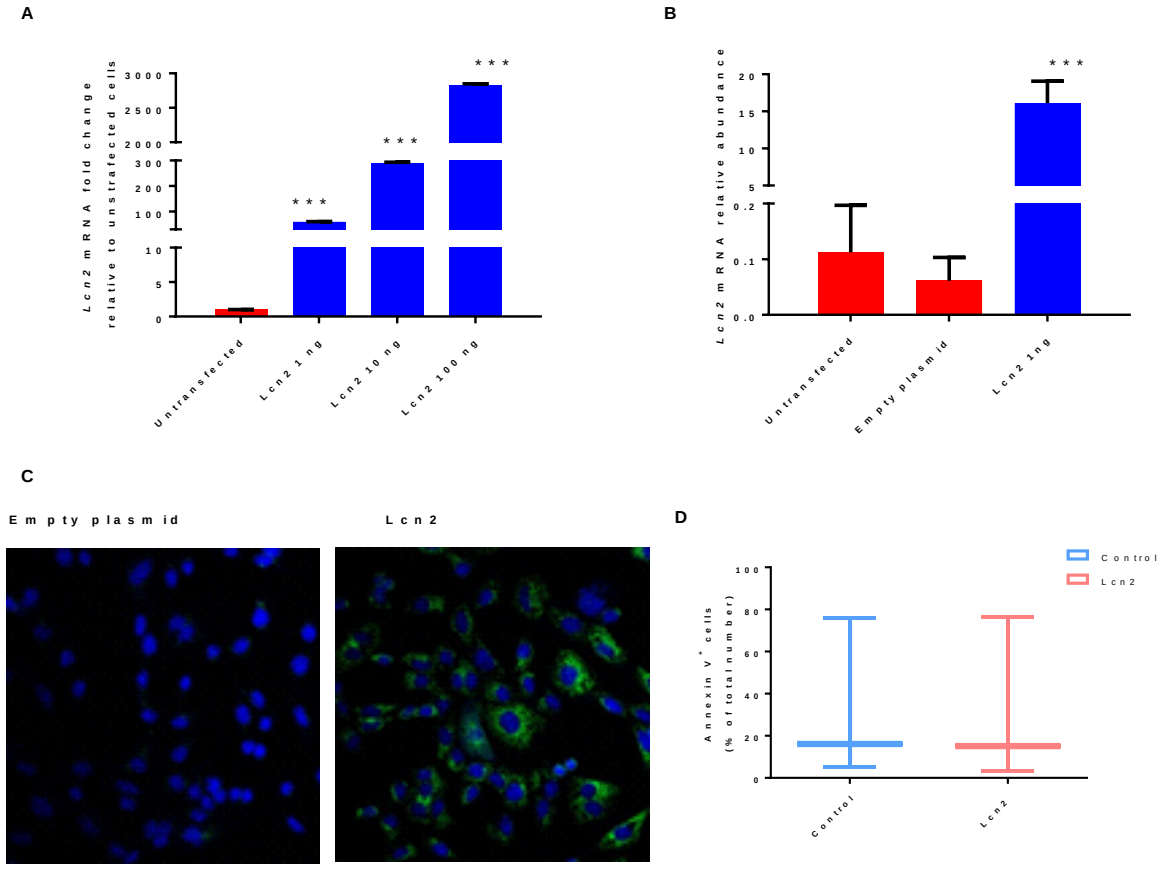

Figure S2. Over-expression of *Lcn2 in vitro*. *Lcn2* was over-expressed in H9c2 cells with the use of a plasmid. **A**, Optimisation of the concentration of Lcn2 plasmid *in vitro*. **B**, There were higher Lcn2 mRNA in cells transfected with LCN2-plasmid. **C**, Over-expression of in cells Lcn2 visualised by immunofluorescence. **D**, There was no difference in apoptotic cells measured by flow cytometry in cells transfected with Lcn2 compared to those transfected with empty plasmid. *** indicates $P<0.001$. Error bars represent standard error of mean.

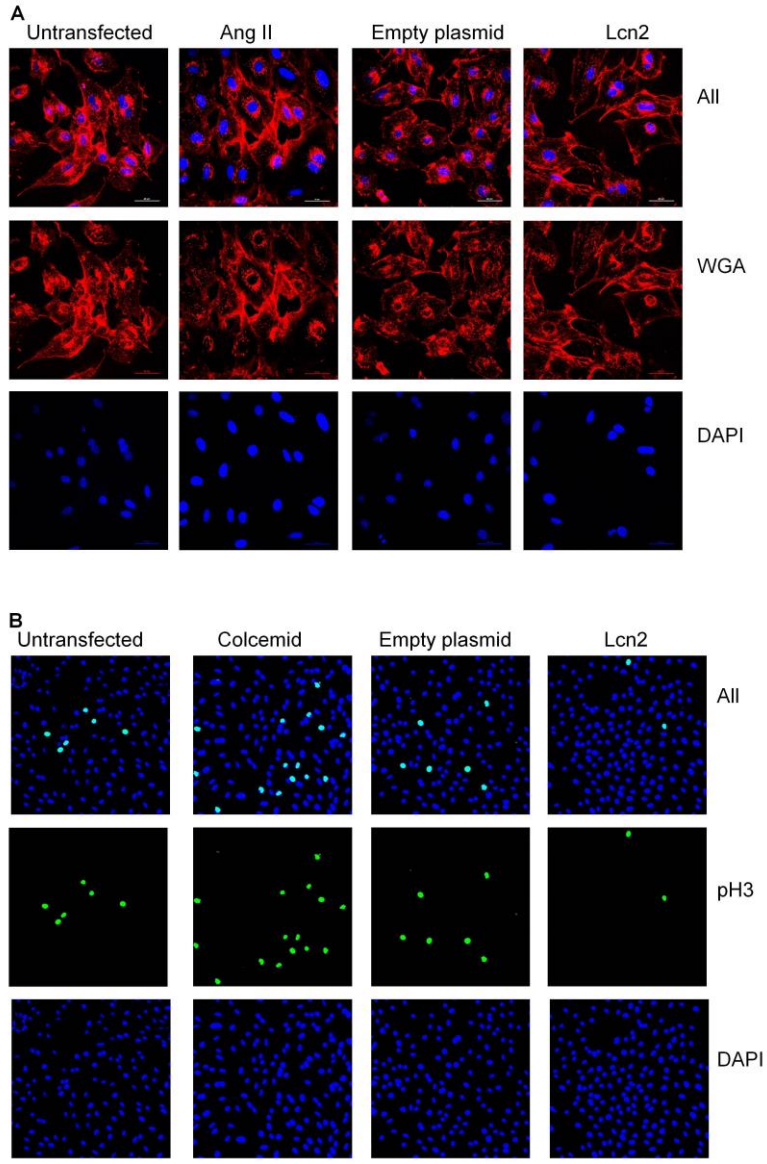

Figure S3. Representative of confocal microscopy images after transfection with Lcn2 plasmid, which provided results for Figure 4 in the main paper. **A**, Wheat-germ agglutinin (WGA, red) and DAPI (blue) staining, used to estimate cell size (400x magnification, scale bar = 60µm). **B**, Phospho-histone H3 (pH3, green) and DAPI (blue), used to estimate cell proliferation and arrest (200x magnification, scale bar = 100µm).

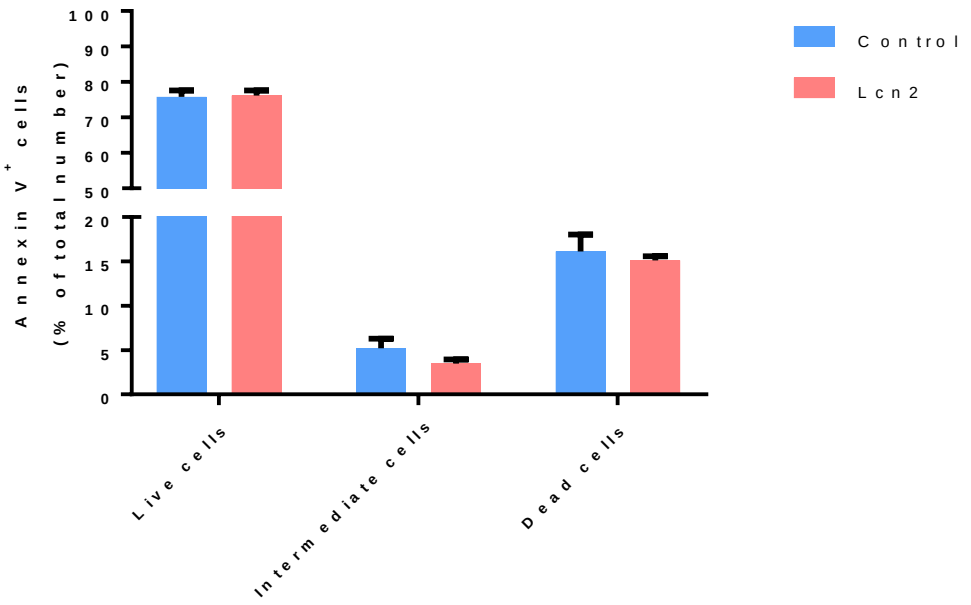

Figure S4. There was no difference in apoptotic cells measured by flow cytometry in cells transfected with Lcn2 compared to those transfected with empty plasmid, demonstrated by annexin V bound to apoptotic cells determined by flow cytometry. Data shown as number of cells as a percentage of the total number of cells. Error bars represent standard error of mean.

Supplemental References:

1. Porrello ER, Bell JR, Schertzer JD, Curl CL, McMullen JR, Mellor KM, Ritchie RH, Lynch GS, Harrap SB, Thomas WG and Delbridge LM. Heritable pathologic cardiac hypertrophy in adulthood is preceded by neonatal cardiac growth restriction. *Am J Physiol Regul Integr Comp Physiol*. 2009;296:R672-80.
2. Harrap SB, Danes VR, Ellis JA, Griffiths CD, Jones EF and Delbridge LM. The hypertrophic heart rat: a new normotensive model of genetic cardiac and cardiomyocyte hypertrophy. *Physiol Genomics*. 2002;9:43-8.
3. Wlodek ME, Mibus A, Tan A, Siebel AL, Owens JA and Moritz KM. Normal lactational environment restores nephron endowment and prevents hypertension after placental restriction in the rat. *J Am Soc Nephrol*. 2007;18:1688-96.
4. Wlodek ME, Westcott K, Siebel AL, Owens JA and Moritz KM. Growth restriction before or after birth reduces nephron number and increases blood pressure in male rats. *Kidney Int*. 2008;74:187-95.
5. Rozen S and Skaletsky H. Primer3 on the WWW for general users and for biologist programmers. *Bioinformatics Methods and Protocols: Methods in Molecular Biology*. 2000: pp. 365-386.
6. Schmittgen TD and Livak KJ. Analyzing real-time PCR data by the comparative C_T method. *Nat Protoc*. 2008;3:1101-8.
7. Flo TH, Smith KD, Sato S, Rodriguez DJ, Holmes MA, Strong RK, Akira S and Aderem A. Lipocalin 2 mediates an innate immune response to bacterial infection by sequestrating iron. *Nature*. 2004;432:917-21.
8. Watkins SJ, Borthwick GM and Arthur HM. The H9C2 cell line and primary neonatal cardiomyocyte cells show similar hypertrophic responses in vitro. *In Vitro Cell Dev Biol Anim*. 2011;47:125-31.
9. Robinson MD, McCarthy DJ and Smyth GK. edgeR: a Bioconductor package for differential expression analysis of digital gene expression data. *Bioinformatics*. 2010;26:139-40.
10. McCarthy DJ, Chen Y and Smyth GK. Differential expression analysis of multifactor RNA-Seq experiments with respect to biological variation. *Nucleic acids research*. 2012;40:4288-97.
11. Robinson MD and Oshlack A. A scaling normalization method for differential expression analysis of RNA-seq data. *Genome biology*. 2010;11.
12. Benjamini Y and Hochberg Y. Controlling the False Discovery Rate - a Practical and Powerful Approach to Multiple Testing. *J Roy Stat Soc B Met*. 1995;57:289-300.
13. Anders S and Huber W. Differential expression analysis for sequence count data. *Genome biology*. 2010;11:R106.
14. Huang da W, Sherman BT and Lempicki RA. Bioinformatics enrichment tools: paths toward the comprehensive functional analysis of large gene lists. *Nucleic Acids Res*. 2009;37:1-13.
15. Huang DW, Sherman BT and Lempicki RA. Systematic and integrative analysis of large gene lists using DAVID bioinformatics resources. *Nat Protoc*. 2009;4:44-57.
16. Zhang H, Meltzer P and Davis S. RCircos: an R package for Circos 2D track plots. *BMC bioinformatics*. 2013;14:244.
17. Porrello ER, Mahmoud AI, Simpson E, Johnson BA, Grinsfelder D, Canseco D, Mammen PP, Rothermel BA, Olson EN and Sadek HA. Regulation of neonatal and adult mammalian heart regeneration by the miR-15 family. *Proc Natl Acad Sci U S A*. 2013;110:187-92.

18. Porrello ER, Johnson BA, Aurora AB, Simpson E, Nam YJ, Matkovich SJ, Dorn GW, 2nd, van Rooij E and Olson EN. MiR-15 family regulates postnatal mitotic arrest of cardiomyocytes. *Circ Res*. 2011;109:670-9.
19. Wai B, Patel SK, Ord M, MacIsaac RJ, Jerums G, Srivastava PM and Burrell LM. Prevalence, predictors and evolution of echocardiographically defined cardiac abnormalities in adults with type 1 diabetes: an observational cohort study. *J Diabetes Complications*. 2014;28:22-8.
20. Lang RM, Bierig M, Devereux RB, Flachskampf FA, Foster E, Pellikka PA, Picard MH, Roman MJ, Seward J, Shanewise JS, Solomon SD, Spencer KT, Sutton MS, Stewart WJ, Chamber Quantification Writing G, American Society of Echocardiography's G, Standards C and European Association of E. Recommendations for chamber quantification: a report from the American Society of Echocardiography's Guidelines and Standards Committee and the Chamber Quantification Writing Group, developed in conjunction with the European Association of Echocardiography, a branch of the European Society of Cardiology. *J Am Soc Echocardiogr*. 2005;18:1440-63.
21. Maragiannis D and Nagueh SF. Echocardiographic evaluation of left ventricular diastolic function: an update. *Curr Cardiol Rep*. 2015;17:3.
22. Peacock WFt, Maisel A, Kim J and Ronco C. Neutrophil gelatinase associated lipocalin in acute kidney injury. *Postgrad Med*. 2013;125:82-93.
23. Raitakari OT, Juonala M, Ronnemaa T, Keltikangas-Jarvinen L, Rasanen L, Pietikainen M, Hutri-Kahonen N, Taittonen L, Jokinen E, Marniemi J, Jula A, Telama R, Kahonen M, Lehtimaki T, Akerblom HK and Viikari JS. Cohort profile: the cardiovascular risk in Young Finns Study. *Int J Epidemiol*. 2008;37:1220-6.
24. Raitoharju E, Seppala I, Oksala N, Lyytikainen LP, Raitakari O, Viikari J, Ala-Korpela M, Soininen P, Kangas AJ, Waldenberger M, Klopp N, Illig T, Leiviska J, Loo BM, Hutri-Kahonen N, Kahonen M, Laaksonen R and Lehtimaki T. Blood microRNA profile associates with the levels of serum lipids and metabolites associated with glucose metabolism and insulin resistance and pinpoints pathways underlying metabolic syndrome: the cardiovascular risk in Young Finns Study. *Mol Cell Endocrinol*. 2014;391:41-9.
25. Smith EN, Chen W, Kahonen M, Kettunen J, Lehtimaki T, Peltonen L, Raitakari OT, Salem RM, Schork NJ, Shaw M, Srinivasan SR, Topol EJ, Viikari JS, Berenson GS and Murray SS. Longitudinal genome-wide association of cardiovascular disease risk factors in the Bogalusa heart study. *PLoS Genet*. 2010;6:e1001094.
26. Wurtz P, Wang Q, Kangas AJ, Richmond RC, Skarp J, Tiainen M, Tynkkynen T, Soininen P, Havulinna AS, Kaakinen M, Viikari JS, Savolainen MJ, Kahonen M, Lehtimaki T, Mannisto S, Blankenberg S, Zeller T, Laitinen J, Pouta A, Mantyselka P, Vanhala M, Elliott P, Pietilainen KH, Ripatti S, Salomaa V, Raitakari OT, Jarvelin MR, Smith GD and Ala-Korpela M. Metabolic signatures of adiposity in young adults: Mendelian randomization analysis and effects of weight change. *PLoS Med*. 2014;11:e1001765.
27. Ruohonen S, Koskenvuo JW, Wendelin-Saarenhovi M, Savontaus M, Kahonen M, Laitinen T, Lehtimaki T, Jokinen E, Viikari J, Juonala M, Taittonen L, Tossavainen P, Kallio M, Bax JJ and Raitakari O. Reference Values for Echocardiography in Middle-Aged Population: The Cardiovascular Risk in Young Finns Study. *Echocardiography*. 2016;33:193-206.
28. Soininen P, Kangas AJ, Wurtz P, Tukiainen T, Tynkkynen T, Laatikainen R, Jarvelin MR, Kahonen M, Lehtimaki T, Viikari J, Raitakari OT, Savolainen MJ and Ala-Korpela M. High-throughput serum NMR metabonomics for cost-effective holistic studies on systemic metabolism. *Analyst*. 2009;134:1781-5.
29. Shi W, Oshlack A and Smyth GK. Optimizing the noise versus bias trade-off for Illumina whole genome expression BeadChips. *Nucleic Acids Res*. 2010;38:e204.

30. Ritchie SC, Wurtz P, Nath AP, Abraham G, Havulinna AS, Fearnley LG, Sarin AP, Kangas AJ, Soininen P, Aalto K, Seppala I, Raitoharju E, Salmi M, Maksimow M, Mannisto S, Kahonen M, Juonala M, Ripatti S, Lehtimaki T, Jalkanen S, Perola M, Raitakari O, Salomaa V, Ala-Korpela M, Kettunen J and Inouye M. The biomarker GlycA is associated with chronic inflammation and predicts long-term risk of severe infection. *Cell Syst*. 2015;1:293-301.
31. Horvath S and Dong J. Geometric interpretation of gene coexpression network analysis. *PLoS Comput Biol*. 2008;4:e1000117.
32. Langfelder P and Horvath S. WGCNA: an R package for weighted correlation network analysis. *BMC Bioinformatics*. 2008;9:559.
33. Teo YY, Inouye M, Small KS, Gwilliam R, Deloukas P, Kwiatkowski DP and Clark TG. A genotype calling algorithm for the Illumina BeadArray platform. *Bioinformatics*. 2007;23:2741-6.